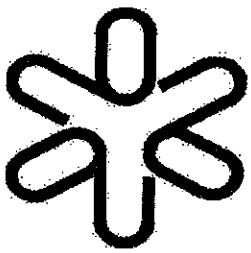

Instituto de Física
Universidade de São Paulo

Glory "in the Shadow of Rainbow"

Ueda, M., Pato, M. P., Hussein, M. S., Takigawa

DEPTO. FÍSICA NUCLEAR

Publicação IF - 1339/98

UNIVERSIDADE DE SÃO PAULO
Instituto de Física
Cidade Universitária
Caixa Postal 66.318
05315-970 - São Paulo - Brasil

DEPARTAMENTO DE FÍSICA NUCLEAR
INSTITUTO DE FÍSICA
UNIVERSIDADE DE SÃO PAULO

IFUSP - DFN/98-014

Glory "in the Shadow of Rainbow"

M. Ueda
M.P. Pato
M.S. Hussein
N. Takigawa

Glory "in the Shadow of Rainbow"

M. Ueda[a,1], M. P. Pato[a], M. S. Hussein[a] and N. Takigawa[a, b]

[a] *Instituto de Física, Universidade de São Paulo*
Caixa Postal 66318, 05389-970 São Paulo SP, Brazil

[b] *Department of Physics, Tohoku University Sendai 980-8578, Japan*

Abstract

We show that the angular distribution of nuclear scattering amplitude behaves like the zeroth order Bessel function with a fixed frequency at extremely forward angles even if there exists no genuine forward glory scattering. A semiclassical interpretation of this behaviour is provided in terms of the effect of scattering in the shadow of nuclear rainbow. We also discuss that the bombarding energy-dependence of the amplitude of the sum-of-difference cross section at very small angles provides a possibility to judge whether the genuine forward nuclear glory scattering is taking place or not.

PACS: 25.70.Bc, 24.10.Ht

Keywords: NUCLEAR REACTIONS nuclear rainbow scattering, forward glory scattering, heavy ion scattering, elastic scattering, sum-of-difference analysis of cross section

[1]e-mail address of the corresponding author: mueda@axpfep1.if.usp.br

1 Introduction

In the beginning of 90s Ostrowski *et al.* [1] claimed that a forward nuclear glory scattering was experimentally observed through the sum-of-difference analysis(SOD analysis) of the very precise data of the cross section of the elastic scattering between two ^{12}C nuclei in a very forward angular region at energies not far above the Coulomb barrier. If this can be confirmed, it will be very useful to comprehend the mechanism of heavy ion collisions at low energies. Also, it will provide a useful information on the interaction between heavy ions or between α particle and nucleus similarly to the nuclear rainbow scattering[2–4] and the backward nuclear glory scattering[5, 6].

The forward nuclear glory scattering is an analogue of a caustic in geometrical optics and the phenomenon that the classical differential cross section *diverges* towards zero degree because of the three-dimensional geometry of the scattering[9]. A characteristic feature is that the nuclear scattering amplitude plotted as a function of the scattering angle behaves like the zeroth order Bessel function with a fixed frequency at forward angles. This behaviour can be understood by a semiclassical theory which leads to an analytic expression of the scattering amplitude. The fixed frequency of the nuclear scattering amplitude at forward angles is associated with the glory angular momentum, which is the angular momentum where the deflection function passes smoothly through zero degree[7].

Until the middle of 80s, it had been thought to be impossible to experimentally observe the forward nuclear glory scattering in heavy ion collisions, because the Rutherford scattering amplitude rapidly diverges at small angles. In order to avoid this difficulty, a generalized optical theorem(GOT)[11–13] was introduced and a method based on it, i.e. the sum-of-difference cross section(SOD or σ_{SOD}) analysis[10], has been invoked to identify the forward nuclear glory scattering and to extract a total reaction cross section from the data at forward angles.

Combining this method and semiclassical analyses, we suggested in our previous papers [14, 15] that the forward nuclear glory scattering is not taking place in almost any heavy ion collisions at low energies even if the forward angular distribution seems to indicate the occurrence

of the forward nuclear glory scattering, and proposed an alternative mechanism, i.e. the shadow effect of a nuclear rainbow, which leads to a very similar angular distribution[15]. In this paper, we present the detailed formalism of this new mechanism, and extend the arguments in Ref. [15].

In Sects. 2 and 3, we briefly explain the forward nuclear glory scattering and the sum-of-difference cross section analysis, respectively. In Sect. 4 we perform a semiclassical analysis of the scattering of α particles from ^{90}Zr to show that no genuine forward glory scattering is taking place, i.e. no glory angular momentum appears in the real space, despite the angular distribution at forward angles behaves very similarly to that for the forward glory scattering. There we remark that a nuclear rainbow appears at a small positive angle. In Sect. 5 we derive a semiclassical formula of the nuclear scattering amplitude for that case, and show that it is given in terms of the zeroth order Bessel function whose frequency is given by the nuclear rainbow angular momentum instead of the glory angular momentum. We show that this analytic formula well explains the main features of the forward angular distribution given by the partial wave sum, thus the origin of the name of the *glory in the shadow of nuclear rainbow.* In Sect. 6 we show that the same formula quantitatively fails to describe a heavier system, i.e. the elastic ^{18}O+^{58}Ni scattering at $E_{Lab.}$ = 63.4 MeV, which could be thought to be an another example of this noble phenomenon and discuss possible origins of the failure, i.e. the validity of the underlying assumptions. In Sect. 7 we argue that the energy dependence of the amplitude of the sum-of-difference cross section at an extremely small angle could be used to extract directly from experimental data a critical energy discriminating two different mechanisms, i.e. the genuine forward nuclear glory scattering and glory in the shadow of nuclear rainbow, which have very similar angular distributions. In Sect. 8 we summarize the paper. An appendix is added to explain the derivation of the semiclassical expression of the nuclear scattering amplitute in the uniform Bessel approximation.

2 Forward nuclear glory scattering

Features of the angular distribution of heavy ion elastic scattering can be well understood based on a semiclassical theory, which leads to various types of analytic expressions of the scattering amplitude depending on the deflection function $\Theta(\lambda)$, which is the scattering angle as a function of the incident angular momentum $\ell(\ \lambda = \ell + 1/2\ )$ or the impact parameter.

Features of the angular distribution of heavy ion elastic scattering can be well understood based on a semiclassical theory by referring to the deflection function $\Theta(\lambda)$, which is the scattering angle as a function of the incident angular momentum $\ell(\ \lambda = \ell + 1/2\ )$ or the impact parameter.

A genuine forward glory scattering occurs if the deflection function smoothly crosses $-2n\pi$ radian, n being an integer, at a finite angular momentum. If there exists a classical trajectory of the projectile that is scattered to zero degree from the target, the classical differential cross section

$$\sigma_{cl}(\theta) = \frac{d\sigma}{d\Omega} = \frac{\lambda}{k^2 \sin\theta}\left\{\frac{d\Theta(\lambda)}{d\lambda}\right\}^{-1} \qquad (2.\ 1)$$

diverges because of the geometrical property of the scattering, i.e. the axial symmetry[9]. This is why the glory scattering is a caustic.

The incident angular momentum where the deflection function crosses zero degree is called a glory angular momentum. Denoting it by $\lambda_g = \ell_g + 1/2$, the angular distribution for the forward nuclear glory scattering can be given analytically in the semiclassical approximation [14] as

$$f_N(\theta) \sim \frac{\lambda_g}{ik}\left(\frac{2\pi\theta}{\sin\theta|\Theta'(\lambda_g)|}\right)^{\frac{1}{2}}|S(\lambda_g)|J_0(\lambda_g\theta)\exp\left[i\left\{2Re\delta(\lambda_g)+\frac{\pi}{4}\right\}\right]\ , \qquad (2.\ 2)$$

where k, $\Theta'(\lambda)$, $|S(\lambda)|$ and $\delta(\lambda)$ are the incident wave number, the derivative of the deflection function with respect to the angular momentum λ, the reflection coefficient and the phase shift of the partial wave $\ell = \lambda - 1/2$, respectively. Eq. (2. 2) shows that the forward nuclear glory scattering is characterized by the angular distribution which behaves like the zeroth order Bessel function with a fixed frequency given by the glory angular momentum.

3 Sum-of-difference cross section

The sum-of-difference cross section is defined by [10–13]

$$\sigma_{SOD} = 2\pi \int_{\theta_0}^{\pi} \left\{ \left(\frac{d\sigma}{d\Omega}\right)_{Ruth.} - \left(\frac{d\sigma}{d\Omega}\right)_{ela.} \right\} \sin\theta d\theta \quad , \tag{3. 1}$$

where $(\frac{d\sigma}{d\Omega})_{Ruth.}$ and $(\frac{d\sigma}{d\Omega})_{ela.}$ are the Rutherford and the elastic scattering differential cross sections, respectively. They are given in terms of the scattering amplitude $f(\theta)$, the Rutherford scattering amplitude $f_C(\theta)$ and the nuclear scattering amplitude $f_N(\theta)$ as

$$\left(\frac{d\sigma}{d\Omega}\right)_{Ruth.} = \mid f_C(\theta) \mid^2 \qquad \left(\frac{d\sigma}{d\Omega}\right)_{ela.} = \mid f(\theta) \mid^2 = \mid f_C(\theta) + f_N(\theta) \mid^2 \tag{3. 2}$$

$$f(\theta) = \frac{1}{2ik} \sum_{\ell} (2\ell+1) \{ e^{i(2\sigma_\ell + 2\delta_\ell^{(N)})} - 1 \} P_\ell(\cos\theta) \tag{3. 3}$$

$$f_N(\theta) = \frac{1}{2ik} \sum_{\ell} (2\ell+1) e^{2i\sigma_\ell} \{ e^{2i\delta_\ell^{(N)}} - 1 \} P_\ell(\cos\theta) \tag{3. 4}$$

$$f_C(\theta) = \frac{1}{2ik} \sum_{\ell} (2\ell+1) \{ e^{2i\sigma_\ell} - 1 \} P_\ell(\cos\theta) = -\frac{\eta}{2k\sin^2(\theta/2)} \exp\left[2i \left(\sigma_0 - \eta \ln \sin\frac{\theta}{2} \right) \right] \quad , \tag{3. 5}$$

where η, σ_ℓ and $\delta_\ell^{(N)}$ are the Sommerfeld parameter, the phase shift of the Rutherford scattering for the ℓth partial wave and that for the scattering by the short-range nuclear interaction, respectively. The latter includes the effect of the deviation of the Coulomb interaction from the point-charge interaction. It has been shown in Ref. [10, 11] that σ_{SOD} is related to the total reaction cross section σ_R and the nuclear scattering amplitude $f_N(\theta)$ as

$$\sigma_{SOD}(\theta_0) = \sigma_R - \frac{4\pi}{k} |f_N(\theta_0)| \sin\left[\arg f_N(\theta_0) - 2\sigma_0 + 2\eta \ln \sin\frac{\theta_0}{2} \right] - \Delta I'(\theta_0) - \Delta N'(\theta_0) \tag{3. 6}$$

with

$$\Delta N'(\theta_0) = 2\pi \int_0^{\theta_0} |f_N(\theta)|^2 \sin\theta d\theta \tag{3. 7}$$

$$\Delta I'(\theta_0) = 4\pi \mathrm{Re}\left[\frac{1}{i\eta} \int_0^{\theta_0} f_C^*(\theta) \frac{df_N(\theta)}{d\theta} (1-\cos\theta) \sin\theta d\theta \right] \quad , \tag{3. 8}$$

where $\Delta N'$ and $\Delta I'$ are correction terms. They become small as θ_0 approaches zero degree and can be ignored in the small angle region which we consider in this paper [10].

The σ_{SOD} rapidly oscillates with θ_0. Its envelope also slowly oscillates around the total reaction cross section. The former arises from the interference between the nuclear and Rutherford scattering amplitudes, and the frequency of the oscillation is mainly determined by the Sommerfeld parameter η. On the other hand, the latter oscillation is caused by the angular distribution of the nuclear scattering amplitude $|f_N(\theta_0)|$ [10]. If one can observe precisely the elastic scattering differential cross section for heavy ion collisions in some forward angular region, the total reaction cross section and the absolute value of the nuclear scattering amplitude at very forward angles can be directly obtained from experimental data through the SOD analysis in a model-independent way, in other words, without going through any optical potentials [1, 16]. The informations on the nuclear scattering amplitude can then be used to learn the scattering mechanism such as the occurrence of forward nuclear glory scattering. Incidentally, if the interest is not to study the forward nuclear glory scattering, it is better to choose lower bombarding energy and the scattering system with a large product of atomic numbers in order to more easily perform the SOD analysis.

4 Semiclassical analysis of elastic α+^{90}Zr scattering

The authors in Ref. [10] discussed the possibility of a forward nuclear glory scattering in the ^{18}O + ^{58}Ni collision at $E_{c.m.}$ = 48.4 MeV based on optical model calculations using a realistic optical potential deduced from the measured elastic scattering angular distribution. They drew the conclusion that a forward nuclear glory scattering is taking place in this scattering by noticing that the envelope of the σ_{SOD} at forward angles behaves like the zeroth order Bessel function with a fixed frequency and that this frequency corresponds to the glory angular momentum, where the classical deflection function calculated for the real part of the optical potential smoothly crosses zero degree. On the other hand, the authors in Ref. [1] studied the elastic scattering between two ^{12}C nuclei at forward angles. They claimed that a forward nuclear glory scattering is taking place in this system based on the observation that $|f_N(\theta)|$ significantly exceeds zero as $\theta_0 \longrightarrow 0$ and exhibits an undulating envelope at forward angles. Refs. [1] and [10] are common in attributing the evidence of the forward nuclear glory scattering to the envelope of the SOD

having the nature of the zeroth order Bessel function with a fixed frequency.

Before we discuss these systems, we present in this section a semiclassical analysis of the α+^{90}Zr elastic scattering at $E_{Lab.} = 40$ MeV in order to discuss whether the envelope of the SOD having the nature of the zeroth order Bessel function with a fixed frequency automatically means the occurrence of the forward nuclear glory scattering. We base our arguments on the optical model analysis using the optical potential which was obtained by fitting the experimental angular distribution[17]. We show that the SOD can have a very similar angular distribution to that in the presence of a forward nuclear glory scattering even if it is actually not taking place.

Fig. 1 shows the angular distribution of the SOD. The solid curve was obtained following the definition of σ_{SOD} given by Eq. (3. 1). On the other hand, the dashed curve was calculated based on the semiclassical formula[1]

$$\sigma_{SOD}(\theta_0) = \sigma_R - \frac{4\pi}{k}|f_N(\theta \simeq 0^\circ)|J_0(\lambda_0\theta)\sin\left\{\arg\, f_N(\theta \simeq 0^\circ) - 2\sigma_0 - 2\eta \ln\sin\frac{\theta}{2}\right\} \qquad (4.\ 1)$$

by assuming that either a forward nuclear glory or some new phenomenon, which is yet unknown but which has a very similar angular distribution, is taking place in this system and ignoring the correction terms in Eq. (3. 6). We used the result of quantum calculations for $f_N(\theta \simeq 0^\circ)$, and calculated the total reaction cross section σ_R by

$$\sigma_R = \frac{\pi}{k^2}\sum_\ell (2\ell+1)(1-|S_\ell|^2) \quad . \qquad (4.\ 2)$$

The frequency parameter λ_0 has been chosen to reproduce the angular distribution of the nuclear scattering amplitude at forward angles with $|f_N(\theta \simeq 0^\circ)|J_0(\lambda_0\theta)$. The resultant value is 19, which coincides with a nuclear rainbow angular momentum as we show later. We see that the solid and the dashed curves agree very well up to 4 degree. This will mean that one can ignore the correction terms in Eq. (3. 6) in this angular region. It also means that the analytic semiclassical formula Eq. (4. 1) works pretty well with an appropriate choice of the frequency parameter λ_0. The important thing in connection with the occurrence of a forward nuclear glory scattering is that the envelope of the SOD can be well represented by the zeroth order Bessel

function with a fixed frequency. The question is whether this necessarily means the occurrence of a forward nuclear glory scattering as has been claimed in Refs. [1] and [10].

In order to answer this question, we show in Fig. 2 the deflection function for this system. The solid curve has been calculated by

$$\Theta(\lambda) = 2\frac{\partial\ \mathrm{Re}\delta(\lambda)}{\partial\lambda} = 2(\mathrm{Re}\ \delta_{\ell+1} - \mathrm{Re}\ \delta_{\ell}) \qquad (4.\ 3)$$

with quantum mechanically calculated phase shifts δ_ℓ. It strongly oscillates in low partial waves, and makes a sudden jump from negative to positive values at the partial wave $\ell \approx 13$ as one increases ℓ. As has been discussed in Ref. [14] the strong oscillation and the sudden jump in the deflection function are caused by the interference between the so called barrier and the internal waves[5, 19]. On the other hand, each deflection function for the barrier(the long-dashed curve) and internal waves(the dot-dashed curve) is a smooth function of the angular momentum[18]. In order to confirm this assertion of the interplay between the barrier and the internal waves, Fig. 3 shows separately the reflection coefficients for the barrier(the long-dashed curve) and the internal(the dot-dashed curve) wave components as functions of the angular momentum. It shows that the barrier and the internal waves dominate low and high partial waves, respectively. The transient partial wave is around 13. Each component is a smooth function of the angular momentum. The total semiclassical scattering amplitude(the solid curve), on the other hand, strongly oscillates for small angular momenta because of the interference between the barrier and the internal waves. Notice that the semiclassical calculations agree very well with quantum mechanical calculations shown by the closed circles.

Returning to Fig. 2, an important observation is that neither the internal nor the barrier wave deflection functions cut zero degree. We therefore conclude that the genuine forward nuclear glory scattering is not taking place in this system. It is then quite puzzling that the angular distribution of the SOD still behaves like that for the forward glory scattering. In next section, we provide an explanation of why the envelope of the SOD, i.e. the forward nuclear scattering amplitude behaves as though there existed a forward nuclear glory scattering even if the deflection function excludes its presence.

In passing, the ratio of the elastic to the Rutherford scattering cross sections is between 0.95 and 1.05 at each angle between 1 and 7 degree. We also calculated the ratio of the sum-of-difference cross section σ_{SOD} to the integrated cross section of the Rutherford scattering from θ_0 to π. We found that the ratio increases from 10^{-3} to 10^{-1} as θ_0 increases from 1 to 10 degree. This gives a measure of the precision required for experimental measurements in order to perform the sum-of-difference cross sections analysis[15].

5 Glory in the shadow of a nuclear rainbow

A clue to understand why the envelope of the SOD behaves as though there were a forward nuclear glory scattering despite its absence can be obtained by noticing that the deflection function for the barrier waves shown in Fig. 2 has a nuclear rainbow at $\lambda \approx 19$, which coincides with λ_0 used to obtain the dashed curve in Fig. 1. For comparison, we show in Fig. 1 the dotted and dot-dashed curves, which represent

$$\sigma_R \pm \frac{4\pi}{k}|f_N(\theta \simeq 0^\circ)|J_0(\lambda_0\theta) \qquad (5.\ 1)$$

with $\lambda_0 = 19$ and 13, respectively. The former is the envelope of the dashed curve. Though it is not easy to judge the superiority of 19 or 13 from the SOD analysis alone, our analysis of the nuclear scattering amplitude at forward angles clearly prefers to the former. Another important issue is which of 19 or 13 better describes the glory minimum, which is the angle where the envelope of the SOD converges. Another important issue is which of 19 or 13 better describes the first node of the envelope of the SOD, which corresponds to the *first rainbow-shadow glory minimum* [15]. It is given by

$$\theta_0 = 3\pi/4\lambda_0 \qquad (5.\ 2)$$

based on Eq. (3. 6) and the properties of the Bessel function[10]. The actual SOD does not clearly show this minimum, but is distorted there because of the effects of the correction terms. We can still see some trace of the glory minimum in Fig. 1. It shows that 19 is better than 13 in this sense too. In this section, we show that the shadow of a nuclear rainbow, which appears

near zero degree, leads to an angular distribution which resembles that for a forward nuclear glory scattering by using the uniform semiclassical approximation[8, 9].

5.1 Integral representation of nuclear scattering amplitude

The scattering amplitude is given by Eq. (3. 3) as the partial wave sum. In order to derive its analytic expression, we first convert it into an integration form by using the Sommerfeld-Watson transformation which leads to the following Poisson sum formula[25],

$$f(\theta) = \frac{1}{ik}\sum_{m=-\infty}^{\infty}\int_0^{\infty} d\lambda e^{2i\pi m\lambda}(-)^m \lambda e^{2i(\sigma(\lambda)+\delta_N(\lambda))} P_{\lambda-1/2}(\cos\theta) \quad , \tag{5. 3}$$

where $\lambda = \ell + 1/2$. We left out the -1 term in Eq. (3. 3) which can be omitted as long as θ is not exactly zero degree [23, 27]. For simplicity, we consider the case where the deflection function $\Theta(\lambda)$ never exceeds $\pm\pi$ so that we can ignore $m \neq 0$ terms in Eq. (5. 3). Furthermore, since we are interested in the forward scattering, we replace the Legendre polynomials by their asymptotic forms using the Bessel function [24]

$$P_{\lambda-1/2}(\cos\theta) \sim \sqrt{\frac{\theta}{\sin\theta}} J_0(\lambda\theta) \qquad (0 \leq \theta \leq \pi - \frac{1}{\lambda}) \tag{5. 4}$$

and use the integral representation of the zeroth order Bessel function in inserting it into Eq. (5. 3). The scattering amplitude is then given by

$$f(\theta) \sim \frac{1}{\pi ik}\left(\frac{\theta}{\sin\theta}\right)^{1/2}\int_0^{\pi} d\phi \int_0^{\infty} d\lambda\lambda |S(\lambda)| e^{i\psi(\lambda,\phi,\theta)} \quad , \tag{5. 5}$$

where

$$\psi(\lambda,\phi,\theta) \equiv 2\delta(\lambda) + \lambda\theta\cos\phi \tag{5. 6}$$

$$|S(\lambda)| = \exp\{-2\mathrm{Im}\delta_N(\lambda)\} \qquad \delta(\lambda) = \sigma(\lambda) + \mathrm{Re}\,\delta_N(\lambda) \quad . \tag{5. 7}$$

In this paper we discuss the case, where the nuclear rainbow angle is positive and close to the zero degree. We approximate the deflection function near the zero degree by a quadratic function around the nuclear rainbow angle θ_{NR},

$$\Theta(\lambda) = \theta_{NR} + \frac{1}{2}\Theta''_{NR}(\lambda - \lambda_{NR})^2 \qquad (\ \theta_{NR} > 0\ ) \tag{5. 8}$$

$$\Theta''_{NR} = \Theta''(\lambda_{NR}) > 0 \qquad \lambda_{NR} = \ell_{NR} + \frac{1}{2} \quad , \tag{5. 9}$$

where ℓ_{NR} and $\Theta''(\lambda)$ are the nuclear rainbow angular momentum and the second derivative of the deflection function with respect to λ, respectively. In the WKB approximation the deflection function $\Theta(\lambda)$ is related to the phase shift by $\Theta(\lambda) = 2\frac{\partial}{\partial\lambda}\delta(\lambda)$ so that the $\psi(\lambda,\phi,\theta)$ in Eq. (5. 6) in the vicinity of the nuclear rainbow angular momentum is given by

$$\psi(\lambda,\phi,\theta) = 2\delta(\lambda_{NR}) + \theta_{NR}(\lambda-\lambda_{NR}) + \frac{1}{3!}\Theta''_{NR}(\lambda-\lambda_{NR})^3 + \lambda\theta\cos\phi \quad . \tag{5. 10}$$

5.2 Evaluation of the λ-integration

We evaluate the integral over λ in Eq. (5. 5) by the stationary phase approximation [23]. The stationary phase angular momenta λ_s are given by

$$\left.\frac{\partial\psi}{\partial\lambda}\right|_{\lambda=\lambda_s} = \theta_{NR} + \frac{1}{2!}\Theta''_{NR}(\lambda_s-\lambda_{NR})^2 + \theta\cos\phi = 0 \tag{5. 11}$$

$$\lambda_s = \lambda_s(\theta,\phi) = \lambda_{NR} \pm i\sqrt{\frac{2(\theta_{NR}+\theta\cos\phi)}{\Theta''_{NR}}} \quad . \tag{5. 12}$$

Eq. (5. 12) is applicable in the angular region smaller than the nuclear rainbow angle, i.e. $\theta \le \theta_{NR}$, where both $\theta_{NR}+\theta\cos\phi$ and Θ''_{NR} are positive. In the following we discard the term with minus sign in front of the i in Eq. (5. 12). The reason will be discussed in Sec. 5-4.

Since the main contribution to the integral over λ now comes from the vicinity of the nuclear rainbow angular momentum λ_{NR}, the scattering amplitude $f(\theta)$ can be regarded as the nuclear scattering amplitude $f_N(\theta)$. The contribution from the Rutherford scattering to forward angles is automatically removed in this stationary phase approximation[14], because the Rutherford scattering to forward angles originates from higher partial waves. Expanding $\psi(\lambda,\phi,\theta)$ in the Taylor series about the stationary phase angular momentum λ_s up to the cubic term, we can write the nuclear scattering amplitude as

$$\begin{aligned} f_N(\theta) &\sim \frac{1}{\pi ik}\sqrt{\frac{\theta}{\sin\theta}}\int_0^\pi d\phi\lambda_s|S(\lambda_s)|e^{2i\delta(\lambda_{NR})} \\ &\times \exp\left\{i\left[\lambda_{NR}\theta\cos\phi + \alpha_s(\theta_{NR}+\theta\cos\phi) + \frac{\alpha_s^3}{2}\Theta''_{NR}\right]\right\} \\ &\times \int_0^\infty d\lambda \exp\left\{i\left[-\frac{\alpha_s^2}{2}\Theta''_{NR}(\lambda-\lambda_{NR}) + \frac{1}{3!}\Theta''_{NR}(\lambda-\lambda_{NR})^3\right]\right\} \quad , \end{aligned} \tag{5. 13}$$

where $\alpha_s = \lambda_s(\theta,\phi) - \lambda_{NR}$. We have also replaced $\lambda|S(\lambda)|$ by its value at the stationary phase angular momentum by assuming that it is a slowly varying function of λ. We now change the

integration variable λ to $x = \lambda - \lambda_{NR}$ and replace the resulting lower limit of the integration from $-\lambda_{NR}$ to $-\infty$. This replacement will be a good approximation because $\psi(\lambda, \phi, \theta)$ changes rapidly for partial waves far from the stationary phase angular momentum and consequently their contributions will almost cancel out each other[23]. The integral over λ in Eq. (5. 13) then becomes an Airy function[24]

$$\int_{-\infty}^{\infty} dx\ e^{i(tx+ax^3)} = 2\pi(3a)^{-1/3}\mathrm{Ai}[(3a)^{-1/3}t] \quad . \tag{5. 14}$$

Thus, the nuclear scattering amplitude is given by the integral over ϕ as,

$$\begin{aligned} f_N(\theta) &\sim \frac{2}{ik}\sqrt{\frac{\theta}{\sin\theta}}\int_0^{\pi} d\phi\ \lambda_s(\theta,\phi)|S(\lambda_s(\theta,\phi))| \\ &\times \exp\left\{i[2\delta(\lambda_{NR}) + \lambda_{NR}\theta\cos\phi + (\theta_{NR}+\theta\cos\phi)\alpha_s(\theta,\phi) + \frac{\Theta''_{NR}}{2}\alpha_s^3(\theta,\phi)]\right\} \\ &\times \left\{\frac{\Theta''_{NR}}{2}\right\}^{-1/3}\mathrm{Ai}\left[\left\{\frac{\Theta''_{NR}}{2}\right\}^{-1/3}(\theta_{NR}+\theta\cos\phi)\right] \quad . \end{aligned} \tag{5. 15}$$

5.3 Semiclassical expression and its limiting case

We evaluate the integral over ϕ in Eq. (5. 15) in the uniform Bessel approximation[9]. The details are given in the appendix. Here we only quote the final analytic expression for the nuclear scattering amplitude,

$$\begin{aligned} f_N(\theta) &\sim \frac{\pi}{ik}\sqrt{\frac{\lambda_{NR}\theta}{\sin\theta}}\left(\frac{\Theta''_{NR}}{2}\right)^{-1/3} e^{2i\delta(\lambda_{NR})}\Big\{A_+(\theta)J_0(\lambda_{NR}\theta) + iA_-(\theta)J_1(\lambda_{NR}\theta)\Big\} \\ A_{\pm}(\theta) &= \sqrt{\lambda_s^-}|S(\lambda_s^-)|\mathrm{Ai}\left[\left(\frac{\Theta''_{NR}}{2}\right)^{-1/3}(\theta_{NR}+\theta)\right] \\ &\pm \sqrt{\lambda_s^+}|S(\lambda_s^+)|\mathrm{Ai}\left[\left(\frac{\Theta''_{NR}}{2}\right)^{-1/3}(\theta_{NR}-\theta)\right] \quad . \end{aligned} \tag{5. 16}$$

Let us now consider the limiting case, where the nuclear rainbow angle θ_{NR} is close to zero degree and the curvature of the deflection function at the nuclear rainbow angular momentum is large. In this case, the imaginary part of the stationary phase angular momentum λ_s given by Eq. (5. 12) is small enough to be ignored and one can approximate both λ_s^+ and λ_s^- by λ_{NR}. Eq. (5. 16) then leads to

$$f_N(\theta) \sim \frac{\pi\lambda_{NR}}{ik}\sqrt{\frac{\theta}{\sin\theta}}\left(\frac{\Theta''_{NR}}{2}\right)^{-1/3}|S(\lambda_{NR})|e^{2i\delta(\lambda_{NR})}\{B_+(\theta)J_0(\lambda_{NR}\theta) + iB_-(\theta)J_1(\lambda_{NR}\theta)\}$$

$$B_{\pm}(\theta) \;=\; \mathrm{Ai}\Big\{\Big(\frac{\Theta''_{NR}}{2}\Big)^{-1/3}(\theta_{NR}+\theta)\Big\} \pm \mathrm{Ai}\Big\{\Big(\frac{\Theta''_{NR}}{2}\Big)^{-1/3}(\theta_{NR}-\theta)\Big\} \quad . \qquad (5.\ 17)$$

We further consider a scattering angle θ which is much smaller than the nuclear rainbow angle θ_{NR}, and approximate $\mathrm{Ai}[a(\theta_{NR}+\theta)] \simeq \mathrm{Ai}[a(\theta_{NR}-\theta)] \simeq \mathrm{Ai}[a\theta_{NR}]$. Thus, the nuclear scattering amplitude in the very forward angular region can be expressed as

$$f_N(\theta) \sim \frac{2\pi\lambda_{NR}}{ik}\sqrt{\frac{\theta}{\sin\theta}}|S(\lambda_{NR})|e^{2i\delta(\lambda_{NR})}\Big(\frac{\Theta''_{NR}}{2}\Big)^{-1/3}\mathrm{Ai}\Big[\Big(\frac{\Theta''_{NR}}{2}\Big)^{-1/3}\theta_{NR}\Big]J_0(\lambda_{NR}\theta) \quad . \quad (5.\ 18)$$

Fig. 4 compares the angular distribution of the modulus of the nuclear scattering amplitude for the α+^{90}Zr elastic scattering at 40 MeV calculated quantum mechanically(the solid curve) and semiclassically based on Eq. (5. 17)(the long-dashed curve). The semiclassical calculations well reproduce the results of quantum mechanical calculations at angles smaller than 11 degree, where a nuclear rainbow appears for the barrier waves. The angular distribution of the nuclear scattering amplitude given by the semiclassical formula Eq. (5. 17) follows the zeroth order Bessel function with a fixed frequency, which is determined by the nuclear rainbow angular momentum. This offers an explanation of the *quasi* glory phenomenon at forward angles in terms of the shadow scattering of a nuclear rainbow appearing near the zero degree.

In Fig. 4 the long-dashed curve systematically underestimates the solid curve in the angular region between the nuclear rainbow and the Coulomb rainbow, which appears at 19 degree. This underestimation will be related to the change of the stationary phase angular momenta λ_s from the dark-side($\theta < 11^\circ$) to the bright-side($\theta > 11^\circ$) regions. In order to describe the nuclear scattering amplitude in the bright-side of the nuclear rainbow, one needs to improve the stationary phase positions and Eq. (5. 17). Beyond the Coulomb rainbow angle the long-dashed curve not only underestimates the magnitude but also the oscillation pattern is different from the solid curve. A proper treatment of the *cubic rainbow*[28] is needed in order to perform a semiclassical analysis including this region.

5.4 Decomposition into the near- and far-side components

In this section we present a semiclassical interpretation of Eq. (5. 16). In the semiclassical theory, the zeroth order Bessel function with a fixed frequency appearing in the analytic expres-

sion of the scattering amplitude is usually thought to be caused by the interference between the far and near side components of the scattering waves[26].

The deflection function for the α+^{90}Zr elastic scattering shown in Fig. 2 appears to have no far side component in the partial wave region which mainly contributes to the forward scattering in question. However, we must note that the stationary phase angular momenta are complex (see Eq. (5. 12)). In other words, the stationary phase positions are hidden in the shadow region of the rainbow angular momentum.

In this subsection we show that the characteristic oscillation pattern due to the shadow of the nuclear rainbow can be expressed in terms of the interference between the far and near side components generalized to the complex angular momentum plane.

We consider a general case instead of introducing the quadratic approximation for the deflection function near the nuclear rainbow angular momentum as has been done in Eq. (5. 11). The stationary phase angular momenta are given by

$$\left.\frac{\partial\psi}{\partial\lambda}\right|_{\lambda=\lambda_s} = \Theta(\lambda_s) + \theta\cos\phi = 0 \quad . \tag{5. 19}$$

As will be discussed in the appendix, the main contributions to the ϕ-integral in the nuclear scattering amplitude come from 0 and π. Hence, Eq. (5. 19) leads to

$$\Theta(\lambda_s^{\mp}) = \begin{cases} -\theta, & \text{for } \phi = 0 \\ +\theta, & \text{for } \phi = \pi \end{cases} \quad . \tag{5. 20}$$

If one can associate these stationary phase angular momenta, $\lambda_s^{\pm}$, with the angular momenta corresponding to the far (near) side components of the scattering waves, the following standard expression of the nuclear scattering amplitude will follow from Eq. (5. 16) in the angular region, where θ is not so small($\theta \gg 1/\lambda_{NR}$) [23, 26].

$$\begin{aligned} f_N(\theta) &= f_N^{(+)}(\theta) + f_N^{(-)}(\theta) \\ f_N^{(\pm)}(\theta) &= \frac{e^{\mp i\frac{\pi}{4}}}{ik\sqrt{\sin\theta}}\left\{\frac{\lambda_s^{\pm}}{|\Theta'(\lambda_s^{\pm})|}\right\}^{1/2}|S(\lambda_s^{\pm})|e^{i\psi(\lambda_s^{\pm},\theta)} \\ \psi(\lambda_s^{\pm},\theta) &= 2\delta(\lambda_s^{\pm}) \mp \lambda_s^{\pm}\theta \quad , \end{aligned} \tag{5. 21}$$

where $f_N^{(+)}(\theta)$ and $f_N^{(-)}(\theta)$ are the near and far side components, respectively.

We can show that this is actually the case in the following way. We first use the following asymptotic forms of the Bessel and the Airy functions[24]

$$J_0(z) \sim \frac{1}{\sqrt{2\pi z}}\{e^{i(z-\frac{\pi}{4})} + e^{-i(z-\frac{\pi}{4})}\} \qquad J_1(z) \sim \frac{-i}{\sqrt{2\pi z}}\{e^{i(z-\frac{\pi}{4})} - e^{-i(z-\frac{\pi}{4})}\} \quad (5.\ 22)$$

$$\mathrm{Ai}(z) \sim \frac{1}{2\sqrt{\pi} z^{1/4}} e^{-\frac{2}{3}z^{3/2}} \ . \quad (5.\ 23)$$

In Eq. (5. 23) we chose the damping form to describe the shadow effect. Substituting these asymptotic forms into Eq. (5. 16), we obtain

$$\begin{aligned} f_N(\theta) &\sim \frac{1}{ik\sqrt{\sin\theta}}\left\{\frac{\lambda_s^-}{[2\Theta''_{NR}(\theta_{NR}+\theta)]^{1/2}}\right\}^{1/2} |S(\lambda_s^-)| e^{i\Psi_-(\theta)} \\ &+ \frac{1}{ik\sqrt{\sin\theta}}\left\{\frac{\lambda_s^+}{[2\Theta''_{NR}(\theta_{NR}-\theta)]^{1/2}}\right\}^{1/2} |S(\lambda_s^+)| e^{i\Psi_+(\theta)} \\ \Psi_\pm(\theta) &= 2\delta(\lambda_{NR}) \mp \lambda_{NR}\theta \pm \frac{\pi}{4} + i\frac{2}{3}\left(\frac{\Theta''_{NR}}{2}\right)^{-1/2} (\theta_{NR} \mp \theta)^{3/2} \ . \end{aligned} \quad (5.\ 24)$$

In deriving the last expression, we took the second derivative of Eq. (5. 10) with respect to λ to obtain

$$\psi''(\lambda, \theta, \phi) = \Theta''_{NR} \cdot (\lambda - \lambda_{NR}) = \Theta'(\lambda) \ . \quad (5.\ 25)$$

The derivative of the deflection function at the stationary phase angular momentum is thus given by

$$\Theta'(\lambda_s) = \Theta''_{NR} \cdot (\lambda_s - \lambda_{NR}) = e^{\pm i\frac{\pi}{2}} \sqrt{2\Theta''_{NR}(\theta_{NR} + \theta\cos\phi)} \ . \quad (5.\ 26)$$

This leads to the factors in front of the absolute values of the scattering matrix in Eq. (5. 24).

We now rewrite the arguments of the exponentials in Eq. (5. 24) using the stationary phase angular momentum $\lambda_s^\pm$. Substituting the expression for the stationary phase position λ_s given by Eq. (5. 12) into Eq. (5. 10), one obtains

$$\psi(\lambda_s, \theta, \phi) = 2\delta(\lambda_{NR}) + \lambda_{NR}\theta\cos\phi \pm i\frac{2}{3}\left(\frac{\Theta''_{NR}}{2}\right)^{-1/2} (\theta_{NR} + \theta\cos\phi)^{3/2} \ . \quad (5.\ 27)$$

The comparison of Eqs. (5. 24) and (5. 27) requires to choose the positive sign in the stationary phase position λ_s in Eq. (5. 12). Note that the upper indices + and − in $\lambda_s^\pm$ originate to distinguish the $\phi = 0$ and $\phi = \pi$ contributions, but are not related to the $\pm$ in Eq. (5. 12). We thus see that Eq. (5. 16) is nothing but the standard expression given by Eq. (5. 21). This

shows that the usual understanding of the oscillation pattern in the forward glory scattering in terms of the interference between the near- and far-side components still holds for the new type of glory phenomenon caused by the shadow of rainbow discussed in this paper.

6 Semiclassical analyses of $^{18}O + ^{58}Ni$ elastic scattering at $E_{c.m.} = 48.4$ MeV

6.1 Influence of absorption potential on the deflection function

We now discuss the $^{18}O + ^{58}Ni$ elastic scattering at $E_{c.m.} = 48.4$ MeV. We assume the same optical potential as that in Ref. [10], which was originally given in Ref. [20]. The corresponding reflection coefficient is shown in Fig. 5 as a function of the angular momentum. The smooth variation from a small value at the zero angular momentum to unity at high angular momenta and the rapid increase around the grazing angular momentum, where the reflection coefficient becomes $1/\sqrt{2}$, indicate that this scattering is dominated by the Coulomb interaction and the strong absorption. Fig. 6 shows the corresponding deflection function. It markedly differs from that shown in Fig. 3 of Ref. [10], which has been obtained by ignoring the imaginary part of the optical potential. Contrary to that in Ref. [10], our deflection function takes 180° at the zero angular momentum and decreases with increasing angular momentum, and does not go through zero degree at any finite angular momentum. The discrepancy between our deflection function and that in Ref. [10] can be attributed to the important role played by the imaginary potential. Fig. 7 shows the deflection function calculated for several strengths of the imaginary potential. As the strength of the imaginary part of the optical potential is reduced, the deflection function approaches the classical one. The strong oscillation appearing in the angular momentum region between 25 and 35 is caused by the interference between the barrier and internal waves. The figure clearly shows that the deflection function under a strong absorption is totally different from that in the absence of absorption. The imaginary part of the optical potential plays a crucial role to reduce the influence of the internal waves and to make the barrier waves dominate[15] in whole angular region. The deflection function for small partial waves changes from internal wave dominated negative value to barrier wave dominated positive value as the absorption gets

stronger. It will be worth noticing that the deflection function shown in Fig. 6 resembles that for the barrier waves which dominate the scattering under strong absorption(see Fig. 5 in Ref. [5].).

6.2 Comparison between quantum mechanical and semiclassical calculations

In Fig. 8 we compare the forward angular distribution of the modulus of the nuclear scattering amplitude calculated quantum mechanically(solid curve) and semiclassically based on Eq. (5. 17)(dashed curve) for the same heavy ion elastic scattering as shown in Figs. 5 and 6. Note that the nuclear and the Coulomb rainbow angles are 46 and 49 degrees, respectively, in our deflection function shown in Fig. 6 which takes the effect of absorption into account. The angular region shown in Fig. 8 therefore corresponds to the dark-side region of the nuclear rainbow. To the contrary, this angular region corresponds to the bright-side of both the Coulomb and the nuclear rainbows for the deflection function calculated classically in Ref. [10] by assuming only the real part of the optical potential(see Fig. 4 in Ref. [10]).

It seems reasonable to consider this angular region by dividing into two parts, i.e. the angular regions smaller and larger than 30 degree, according to the behaviour of the angular distribution obtained by the quantum mechanical calculations. The large angle region, where a subtle undulation appears, is characterized by a rather steep increase of the modulus of the nuclear scattering amplitude with the scattering angle. The semiclassical calculations(dashed curve) well reproduce the magnitude of the quantum mechanical calculations(solid curve) in this angular region, so that the nuclear scattering amplitude at angles between 30 degree and the nuclear rainbow angle can be interpreted as the shadow of the nuclear rainbow scattering.

On the other hand, the strong oscillation in the solid curve at small angles could also be interpreted in terms of the glory in the shadow of rainbow. In fact the dashed curve which has been calculated based on this idea, i.e. Eq. (5. 17), has a very similar oscillation pattern with a frequency corresponding to the nuclear rainbow angular momentum $\lambda \approx 34$(see Fig. 6). A problem is, however, it severely underestimates the magnitude compared to the solid curve. The magnitude of the semiclassical amplitude is only about 30 % of that of the quantum

mechanical one at around zero degree. Two reasons can be considered for this discrepancy. One is that the approximation $\lambda_s^{\pm}(\theta) \approx \lambda_{NR}$ used to obtain Eq. (5. 17) is not applicable to this forward scattering. The other is a diffraction effect[27], which has been ignored in deriving the semiclassical formulae Eqs. (5. 16) and (5. 17). We discuss the former problem in the next subsection.

6.3 Validity of the approximation $\lambda_s^{\pm} \approx \lambda_{NR}$

As shown in Eq. (5. 12), the stationary phase angular momenta $\lambda_s^{\pm}(\theta)$ differ from λ_{NR} by a purely imaginary quantity which is determined by the nuclear rainbow angle and the curvature of the deflection function at the nuclear rainbow angular momentum. Therefore $\lambda_s^{\pm}$ significantly deviates from λ_{NR} if the nuclear rainbow angle is large and/or if the curvature of the deflection function at the nuclear rainbow angular momentum is small. For the α+^{90}Zr elastic scattering at 40 MeV discussed in Sects. 4 and 5, the nuclear rainbow angle θ_{NR} and the curvature of the deflection function at the nuclear rainbow angular momentum $\Theta''(\lambda_{NR})$ are 11.5 ° and 0.136, respectively. The modulus of the deviation of $\lambda_s^{\pm}$ from λ_{NR} at the zero degree, where it gets maximum, is 1.71 and its ratio to λ_{NR} is 0.090. In the ^{18}O+^{58}Ni elastic scattering at $E_{c.m.}$ = 48.4 MeV, θ_{NR} and $\Theta''(\lambda_{NR})$ are 46.8° and 0.036, respectively. Hence, deviation of $\lambda_s^{\pm}(0°)$ from λ_{NR} is large. Its absolute value and the ratio to λ_{NR} are 6.73 and 0.196, respectively.

The success of our semiclassical calculation to reproduce the quantum mechanical calculations at forward angles for the α+^{90}Zr elastic scattering at $E_{Lab.}$ = 40 MeV suggests that one can replace $\lambda_s^{\pm}$ by λ_R if the ratio $|\lambda_s^{\pm} - \lambda_R|/\lambda_R$ is less than about 0.1. This surmise is consistent with the observation that the semiclassical formula given by Eq. (5. 17) well reproduces the magnitude of the nuclear scattering amplitude for the ^{18}O + ^{58}Ni elastic scattering in the angular region between 30° and the nuclear rainbow angle, where the ratio $|\lambda_s^{\pm} - \lambda_R|/\lambda_R$ is less than 0.12. How to evaluate the $\sqrt{\lambda_s^{\mp}}|S(\lambda_s^{\pm})|$ for complex $\lambda_s^{\pm}$ is an open question. Incidentally, this is related to the problem of deviation of the phase of SOD between the semiclassical and quantum mechanical calculations discussed in Ref. [15].

In this section we discussed the forward nuclear scattering amplitude for the ^{18}O + ^{58}Ni

elastic scattering at $E_{c.m.}$ = 48.4 MeV. In this scattering, the strong Coulomb repulsion pushes the nuclear rainbow angle far away from the zero degree and also reduce the curvature of the deflection function at the nuclear rainbow angle. Consequently, *the glory in the shadow of rainbow* is suppressed. It is better to choose the scattering between relatively light heavy ions or between α particles and heavy-nuclei, which has a relatively weak Coulomb repulsion, to observe *the glory in the shadow of rainbow.*

7 Energy-dependence of the forward nuclear glory scattering

It is an interesting question to look for a method to distinguish the genuine forward nuclear glory scattering from other mechanisms which lead to a resembling angular distribution at a given energy. We have already mentioned that low energy collisions, where there exist three active classical turning points for each partial wave, cannot be simply understood as a forward glory scattering, because the interference between the internal and barrier waves leads to a complicated oscillation in the total deflection function. Another interesting observation is that the nuclear rainbow angle gradually decreases with increasing bombarding energy and becomes negative at some critical energy on causing glory angular momenta if one plots the smooth part of the deflection function. This behaviour is demonstrated in Fig. 9, where we show the smooth part of the deflection function for the $\alpha + {}^{90}$Zr elastic scattering at several bombarding energies. It was obtained by first calculating the deflection function quantum mechanically for an optical potential scattering and then keeping only the smooth part at high angular momenta. The top and the bottom figures have been obtained by using the energy-dependent phenomenological and energy-independent optical potentials shown in Table 1, respectively. The former was determined by fitting the experimental angular distribution of the elastic scattering [17] at each energy up to $E_{Lab.}$=141.7 MeV, and by extrapolating the potential parameters to $E_{Lab.}$=200 MeV[18]. The latter was identified with the phenomenological optical potential at 99.5 MeV.

We obtained the deflection function for the barrier waves practically in this way from quantum mechanical calculations. The deflection function for $E_{Lab.}$ = 200 MeV is smooth from the beginning reflecting the fact that there exists only one physically important turning point for

each partial wave, and the decomposition into the barrier and internal waves looses meaning at this energy. The figure shows that the nuclear rainbow angle reaches zero degree, in other words a forward nuclear glory shows up in the classical deflection function, at about 80 MeV for the first time as the bombarding energy is increased. The deflection functions for the energy-dependent and the energy-independent potentials have a similar global behaviour. Fig. 9 indicates that the bombarding energy dependence of the amplitude of the SOD might become a criterion to distinguish the genuine forward nuclear glory scattering from other mechanisms leading to a similar angular distribution. In this section, we address to this possibility.

When the forward nuclear glory scattering takes place, the amplitude of the SOD is given semiclassically by

$$\frac{4\pi|f_N(0^\circ)|}{k} = \frac{4\pi}{k}\frac{\lambda_g}{k}\sqrt{\frac{2\pi}{|\Theta'(\lambda_g)|}}|S(\lambda_g)| \quad , \tag{7. 1}$$

where λ_g, $|S(\lambda)|$ and $\Theta'(\lambda)$ are the glory angular momentum, the reflection coefficient as a function of the angular momentum λ and the derivative of the deflection function with respect to λ, respectively. Fig. 10−A(the top figure) shows the energy-dependence of the glory angular momentum λ_g. Closed and open circles were obtained from the corresponding deflection functions in the top and the bottom of Fig. 9, respectively. Closed and open diamonds denote the grazing angular momenta $\lambda_{gr} = \ell_{gr} + 1/2$, for which $|S(\lambda_{gr})| = 1/\sqrt{2}$, in quantum mechanical calculations with the energy-dependent and the energy-independent optical potentials, respectively. In addition to the 7 energies in Fig. 9, the figure contains two higher energy points, i.e. at 250 and 300 MeV.

It is interesting to notice that the grazing angular momentum is almost the same for the energy-dependent and energy-independent optical potentials, while the glory angular momentum noticeably differs for two potentials. However, the deviation between the glory and the grazing angular momenta are within 5% even for the energy independent potential. Thus, we approximate the glory angular momentum by the grazing angular momentum, i.e. $\lambda_g \simeq \lambda_{gr}$. We assume that the grazing angular momentum is roughly given by

$$kR_B = \eta + \sqrt{\eta^2 + \lambda_{gr}^2} \quad , \tag{7. 2}$$

where η and R_B are the Sommerfeld parameter and the relative distance between the α-particle and ^{90}Zr at the position of the Coulomb barrier, respectively. Eq. (7. 2) leads to

$$\lambda_{gr} = kR_B\left(1 - \frac{V_B}{E}\right)^{1/2} \quad , \tag{7. 3}$$

where E and $V_B = Z_P Z_T e^2/R_B$ are the bombarding energy in the center of mass system and the Coulomb barrier height at R_B, respectively. $Z_P Z_T$ is the product of the atomic numbers of the projectile and target. If the bombarding energy is high enough to ignore V_B/E, the grazing and the glory angular momentum will be proportional to k as has been argued in Refs. [21, 22].

The dashed curve in Fig. 10−A has been obtained based on Eq. (7. 3), by using R_B = 9.43 fm and V_B = 11.2 MeV for the optical potential at $E_{Lab.}$ = 99.5 MeV(k = 4.19 fm^{-1}), respectively. Although the dashed curve has a similar energy-dependence as open circles, the former significantly overestimates the latter. In order to obtain the glory angular momentum with the correct magnitude shown in Fig. 10−A, we introduce an effective radius R_g in such a way that λ_g at 99.5 MeV is correctly reproduced when λ_{gr} and R_B in Eq. (7. 2) are replaced by λ_g and R_g. We then keep R_g energy independent and use Eq. (7. 2) to obtain the energy dependence of the glory angular momentum with the correct magnitude. The glory angular momentum thus obtained is given by

$$\lambda_g = kR_B x^{-1}\left(1 - x\frac{V_B}{E}\right)^{1/2} \qquad x = \frac{R_B}{R_g} \tag{7. 4}$$

and is shown by the solid curve in Fig. 10−A, which agrees very well with open circles. In passing, we notice that Fig. 3 in Ref. [5] shows that the backward glory angular momentum and the nuclear rainbow angular momentum are very close to the grazing angular momentum and that they have a very similar energy-dependence.

It is not easy to derive an analytic expression for the derivative of the deflection function directly from the semiclassical phase shift in WKB approximation for general cases. One of the authors(M. S. H.) derived in Ref. [22] the following analytic expression of the derivative of the deflection function at the glory angular momentum $\Theta'(\lambda_g)$

$$|\Theta'(\lambda_g)| \approx \frac{Z_P Z_T e^2}{Ea\lambda_g} \tag{7. 5}$$

by using a high-energy approximation for the nuclear phase shift and by assuming a constant value for the glory impact parmater $b_g = \lambda_g/k$. In Eq. (7. 5) a is the surface diffuseness parameter of the real part of the optical potential whose shape is assumed to be of Woods-Saxon type. Eq. (7. 5) indicates that $\Theta'(\lambda_g)$ has k^{-3}-dependence. Replacing λ_g in Eq. (7. 5) by Eqs. (7. 3) and (7. 4), we obtain two alternative expressions for the r.h.s. of Eq. (7. 5)

$$\frac{1}{ka}\frac{V_B}{E}\left(1-\frac{V_B}{E}\right)^{-1/2} \tag{7. 6}$$

and

$$\frac{1}{ka}x^{-1}\frac{V_B}{E}\left(1-x\frac{V_B}{E}\right)^{-1/2} \quad , \tag{7. 7}$$

respectively. Fig. 10−B shows the energy-dependence of the derivative of the deflection function at the glory angular momentum. Closed and open circles have been calculated quantum mechanically for the energy-dependent and independent optical potentials, respectively. They are almost the same at each energy. The dashed and solid curves are given by Eqs. (7. 6) and (7. 7), respectively. Both the solid and dashed curves reproduce very well the closed and the open circles, though the latter is better, except for those at 79.5 MeV, which seems to lie on the borderline. This means that Eq. (7. 5) well describes the energy-dependence of the derivative of the deflection function at the glory angular momentum. Also, both the solid and the dashed curves behave like ck^{-3}(dotted curve), c being a constant.

Fig. 10−C shows the energy-dependence of the reflection coefficient at the glory angular momentum $|S(\lambda_g)|$. Closed and open circles have been calculated quantum mechanically for the energy-dependent and independent optical potentials, respectively. If the approximation $\lambda_g \simeq \lambda_{gr}$ is adequate, the reflection coefficient at the glory angular momentum is expected to have a very weak energy-dependnece around $1/\sqrt{2}$(dashed curve). On the other hand, it is also expected to have a $\exp(-c/k)$-dependence, c being a constant(dotted curve), in the high-energy approximation[22]. However, neither the closed circles nor the open ones obey these expectations concerning the energy-dependence. We therefore fitted the open circles by the following two functions

$$|S(\lambda_g)| = \exp\left(aE^b\left(1-\frac{V_B}{E}\right)^c\right) \tag{7. 8}$$

and

$$|S(\lambda_g)| = \exp\left(a' E^{b'}\left(1 - x\frac{V_B}{E}\right)^{c'}\right) \quad . \tag{7. 9}$$

The obtained parameters are (a, b, c) = (0.654, -0.335, -6.35) and (a', b', c') = (0.675, -0.339, -5.58). They are almost the same, so that we draw in Fig. 10−C only one curve(the solid curve) to represent them.

Substituting $|S(\lambda_g)| = 1/\sqrt{2}$, Eqs. (7. 3) and (7. 6) into Eq. (7. 1) in the cases where the approximation $\lambda_g \simeq \lambda_{gr}$ is reasonable, we obtain the analytic expression for the forward amplitude of the SOD as follows

$$4\pi\frac{|f_N(0)|}{k} \approx 4\pi R_B\left(\frac{\hbar\pi a}{\sqrt{2\mu V_B}}\right)^{1/2} E^{1/4}\left(1 - \frac{V_B}{E}\right)^{3/4} \propto E^{1/4}\left(1 - \frac{V_B}{E}\right)^{3/4} \quad , \tag{7. 10}$$

where μ is the reduced mass. On the other hand, substituting Eqs. (7. 4), (7. 7) and (7. 9) into Eq. (7. 1) when $\lambda_g \neq \lambda_{gr}$, we obtain the following modified analytic expression for the forward amplitude of the SOD

$$\begin{aligned} 4\pi\frac{|f_N(0)|}{k} &\approx \frac{4\pi R_B}{x^{3/2}}\left(\frac{2\hbar\pi a}{\sqrt{2\mu V_B}}\right)^{1/2} E^{1/4}\left(1 - x\frac{V_B}{E}\right)^{3/4} |S(\lambda_g)| \\ &\propto E^{1/4}\left(1 - x\frac{V_B}{E}\right)^{3/4} |S(\lambda_g)| \quad . \end{aligned} \tag{7. 11}$$

Eq. (7. 11) reduces to Eq. (7. 10) if x in Eq. (7. 11) is nearly equal to 1. Furthermore, if V_B/E is small enough to be ignored, Eqs. (7. 10) and (7. 11) lead to $E^{1/4}$-dependence of the forward amplitude of the SOD, which has once been obtained by using the high-energy approximation in Ref. [22].

We now compare the predictions of the analytic expressions Eqs. (7. 10) and (7. 11) with the direct quantum mechanical calculations. Fig. 11 shows the bombarding energy-dependence of the amplitude of the SOD at very forward angles for α+^{90}Zr elastic scattering. Closed and open circles have been calculated quantum mechanically with the energy-dependent and the energy-independent optical potentials, respectively. The dashed and the solid curves are given by Eqs. (7. 10) and (7. 11), respectively. Despite that the solid curve has been obtained by using λ_g, $|\Theta'(\lambda_g)|$ and $|S(\lambda_g)|$ which can reproduce respective quantum mechanical calculations,

it significantly overestimates open circles at energies higher than 90 MeV, where the forward nuclear glory scattering is actually taking place. Moreover, the ratio of the deviation between the solid curve and the open circles to the latter increases from 8% to 28% when the bombarding energy is increased from 100 MeV to 300 MeV. This suggests that Eq. (7. 1) derived in the stationary phase approximation cannot give the correct magnitude of the forward nuclear glory scattering amplitude and is not adequate to make a quantitative analysis. This failure could be understood as follows. The analytic expression Eq. (2. 2) has been obtained in the stationary phase approximation based on the assumption that the deflection function around zero degree can be well approximated by a linear function as

$$\Theta(\lambda) = \Theta'(\lambda_g)(\lambda - \lambda_g) \quad . \tag{7. 12}$$

$\Theta'(\lambda_g)$ contains the information of how many partial waves around the glory angular momentum contribute to the forward scattering causing a caustic. As Figs. 9 and 10−B show, the slope of the deflection function at the glory angular momentum decreases with increasing bombarding energy, and more partial waves around the glory angular momentum contribute to the very forward scattering. However, the deflection function deviates from Eq. (7. 12) in heavy ion scatterings and scatterings between α-particles and nuclei at high angular momenta, because the Coulomb rainbow angle becomes close to zero degree. A reason why Eq. (7. 1) gives systematically larger SOD amplitude than the quantum-mechanical calculations(open circles) will be that Eq. (7. 1) includes false contributions from very high partial waves which should not play a role in the actual forward nuclear glory scattering. In order to make a quantitative analysis of the forward nuclear glory scattering amplitude, we need a more elaborate analytic expression which takes the above effect into account.

Another problem of Eq. (7. 11), which led to the solid curve in Fig. 11, is a slightly inconsistent treatment of λ_g/k, $\Theta'(\lambda_g)$ and $|S(\lambda_g)|$. Though the energy dependence of the former two has be treated based on the approximation $\lambda_g \approx \lambda_{gr}$, we used the more detailed energy dependence for λ_g. The dashed curve in Fig. 11 is more consistent in that respect. An interesting observation is that the energy dependence of the dashed curve looks similar to that

of the open circles, though the magnitude is very different.

We now reanalyse by keeping only the energy dependence of Eq. (7. 10). The dotted and dot-dashed curves in Fig. 11 have been obtained by assuming $c_1 E^{1/4}(1 - V_B/E)^{3/4}$ and $c_0 E^{1/4}$ for $|f_N(0)/k|$. The coefficients c_1 and c_0 have been determined to reproduce the open circle at 99.5 MeV. The upper part of Fig. 12 shows how the value of c_1 varies when one changes the normalization point from 99.5 MeV to the other energies. The lower part of Fig. 12 shows the corresponding χ^2 values defined by

$$\sum_i \left| \frac{|f_N(0)/k| - c_1 E^{1/4}(1 - V_B/E)^{3/4}}{f_N(0)/k} \right|_i^2 , \qquad (7.\ 13)$$

where the sum over i runs over all data points. Fig. 12 clearly shows that the reaction mechanism changes around 80 MeV. It is interesting to notice that this energy is close to the first kind of critical energy discussed in Ref. [18], where the corresponding grazing partial wave looses its potential pocket. Judging from these analyses, we consider that the bombarding energy-dependence of the forward amplitude of the SOD gives a criterion of the occurrence of the genuine forward nuclear glory scattering.

8 Summary

We discussed the nuclear scattering amplitude in elastic heavy ion scattering and in the scattering of α particles from nuclei at extremely forward angles through the SOD analysis. We showed that the envelope of the SOD in the very forward angular region, or the angular distribution of the nuclear scattering amplitude, behaves like the zeroth order Bessel function with a fixed frequency even if no forward nuclear glory scattering is taking place in the classical sense.

For the α+^{90}Zr elastic scattering, we gave a semiclassical interpretation of this new phenomenon in terms of the shadow effect of the nuclear rainbow scattering. We named this *glory in the shadow of nuclear rainbow* and derived an analytic expression of the corresponding nuclear scattering amplitude in the uniform stationary phase approximation Eq. (5. 17). We also showed that the standard interpretation of the characteristic oscillation pattern in terms of the

interference between the far and near side components holds for this phenomenon, too.

The elastic $^{18}O + {}^{58}Ni$ scattering shows a similar behaviour of the nuclear scattering amplitude, and could be understood as another example of this new phenomena. However, the same semiclassical formula did not work so well compared to the case of $\alpha+^{90}Zr$ elastic scattering. We showed that the absorption plays a crucial role in this scattering. A simultaneous treatment of the refractive and diffractive effects will be needed to properly describe this system. Another reason of the failure of the present semiclassical formula for this system is that the strong Coulomb repulsion pushes the nuclear rainbow angle far away from the zero degree and reduces the curvature of the deflection function at nuclear rainbow angular momentum λ_{NR}. They invalidate the approximation to replace the complex stationary phase angular momentum given by Eq. (5. 12) with λ_{NR}, which has been used in deriving Eq. (5. 17).

The analysis of these two systems implies that scattering systems with a weak Coulomb repulsion is preferable if one wishes to extract informations on the nuclear interaction between heavy ions or between α particles and nuclei through the SOD analysis. We should notice also that a large value of Sommerfeld parameter facilitates the SOD analysis. Consequently, the scattering between light heavy ions or between α particles and heavy-nuclei at energies not far above the Coulomb barrier are good candidates to observe the *glory in the shadow of nuclear rainbow* .

Our study shows that the angular distribution which behaves like the zeroth order Bessel function with a fixed frequency cannot be a definite evidence of the genuine forward nuclear glory scattering. A natural question is then how one can distinguish the genuine forward nuclear glory scattering from the other mechanism leading to a similar angular distribution. In this connection, we studied the energy dependence of the amplitude of the SOD at very forward angles and of the corresponding deflection function by taking the $\alpha+^{90}Zr$ elastic scattering from 40 to 300 MeV as an example. We have shown that one can extract a critical energy, above which the typical angular distribution having the properties of the zeroth order Bessel function can be associated with the genuine forward nuclear glory scattering, by studying the energy dependence of the amplitude of the SOD at extremely forward angles.

Acknowledgments

M.U. and N.T. thank the late Prof. Dr. T. Yamaya and Dr. H. Ishiyama for useful discussions. M.U. acknowledges support from Fundaçao de Amparo á Pesquisa do Estado de São Paulo (FAPESP). M.P.P and M.S.H acknowledge support from the Brazilian National Research Council (CNPq) and FAPESP. This work is also supported by the Monbusho International Scientific Research Program: Joint Research: contract number 09044051; and in part by the Grant-in-Aid for General Scientific Research, Contract No. 08640380 from the Japanese Ministry of Education, Science and Culture.

Appendix: Derivation of the semiclassical formula for the nuclear scattering amplitude Eq. (5. 16)

In this appendix, we derive the semiclassical expression of the nuclear scattering amplitude given by Eq. (5. 16) in the uniform Bessel approximation.

The first step is to change the variable ϕ and the argument of the exponential in Eq. (5. 15) to a new variable φ and a simpler function by one-to-one mapping,

$$2\delta(\lambda_{NR}) + \lambda_{NR}\theta\cos\phi + (\theta_{NR} + \theta\cos\phi)\alpha_s(\theta,\phi) + \frac{\Theta''_{NR}}{2}\alpha_s^3(\theta,\phi) \longrightarrow a(\theta) + b(\theta)\cos\varphi \quad . \quad \text{(A. 1)}$$

The mapping is done such that the r.h.s. of Eq. (A. 1) has the same structure of stationary positions as the l.h.s., and that each end of the l.h.s. in Eq. (A. 1) is mapped on the corresponding end of the r.h.s. These requirements impose the following relationships;

$$\phi(\varphi = 0) = 0 \qquad \phi(\varphi = \pi) = \pi \qquad \text{(A. 2)}$$

$$2\delta(\lambda_{NR}) \pm \lambda_{NR}\theta + (\theta_{NR} \pm \theta)\alpha_s^{\mp}(\theta) + \frac{\Theta''_{NR}}{2}\{\alpha_s^{\mp}(\theta)\}^3 = a(\theta) \pm b(\theta) \quad , \qquad \text{(A. 3)}$$

where

$$\begin{aligned} \alpha_s^{\mp}(\theta) &= \lambda_s^{\mp} - \lambda_{NR} \\ \lambda_s^{-} &= \lambda_s(\theta, \phi = 0) \qquad \lambda_s^{+} = \lambda_s(\theta, \phi = \pi) \quad . \end{aligned} \qquad \text{(A. 4)}$$

Using Eqs. (A. 3) and (5. 12),

$$\begin{aligned} a(\theta) \pm b(\theta) &= 2\delta(\lambda_{NR}) \pm \lambda_{NR}\theta + \alpha_s^{\mp}\left\{ \frac{\Theta''_{NR}}{2}(\alpha_s^{\mp})^2 + (\theta_{NR} \pm \theta) \right\} \\ &= 2\delta(\lambda_{NR}) \pm \lambda_{NR}\theta \ . \end{aligned} \tag{A. 5}$$

Thus, one can obtain the functions $a(\theta)$ and $b(\theta)$ as

$$a(\theta) = 2\delta(\lambda_{NR}) \qquad b(\theta) = \lambda_{NR}\theta \ . \tag{A. 6}$$

Eq. (5. 15) now reads,

$$f_N(\theta) \sim \frac{2}{ik}\sqrt{\frac{\theta}{\sin\theta}}\left(\frac{\Theta''_{NR}}{2}\right)^{-1/3} e^{2i\delta(\lambda_{NR})} \int_0^{\pi} d\varphi \ e^{i\lambda_{NR}\theta\cos\varphi} G(\theta, \phi(\varphi)) \tag{A. 7}$$

with

$$\begin{aligned} &G\Big(\theta, \phi(\varphi)\Big) = \\ &\left(\frac{d\phi}{d\varphi}\right)\lambda_s(\theta, \phi(\varphi))|S(\lambda_s(\theta, \phi(\varphi)))|\mathrm{Ai}\left[\left(\frac{\Theta''_{NR}}{2}\right)^{-1/3}(\theta_{NR} + \theta\cos\phi(\varphi))\right] \ . \end{aligned} \tag{A. 8}$$

The next step is to replace the function $G(\theta, \phi(\varphi))$ by a suitable simple function [9, 28],

$$G(\theta, \phi(\varphi)) = p(\theta) + q(\theta)\cos\varphi + h(\varphi, \theta)\sin\varphi \ . \tag{A. 9}$$

The integral in Eq. (A. 7) then becomes

$$\int_0^{\pi} d\varphi \ \{p(\theta) + q(\theta)\cos\varphi + h(\varphi, \theta)\sin\varphi\} e^{i\lambda_{NR}\theta\cos\varphi} \ . \tag{A. 10}$$

The first two terms in Eq. (A. 10) can be analytically calculated and expressed in terms of the zeroth and first order Bessel functions, respectively[24],

$$p(\theta)\int_0^{\pi} d\varphi e^{i\lambda_{NR}\theta\cos\varphi} = \pi p(\theta)J_0(\lambda_{NR}\theta) \tag{A. 11}$$

$$q(\theta)\int_0^{\pi} d\varphi\cos\varphi \ e^{i\lambda_{NR}\theta\cos\varphi} = i\pi q(\theta)J_1(\lambda_{NR}\theta) \ . \tag{A. 12}$$

We evaluate the third term in Eq. (A. 10) in the stationary phase approximation,

$$\int_0^{\pi} d\varphi h(\varphi, \theta)\sin\varphi e^{i\lambda_{NR}\theta\cos\varphi} \propto h(\varphi_0, \theta)\sin\varphi_0 e^{i\lambda_{NR}\theta\cos\varphi_0} \ , \tag{A. 13}$$

where φ_0 is the stationary phase position and is determined by

$$\frac{d}{d\varphi}\{\lambda_{NR}\theta\cos\varphi\} = -\lambda_{NR}\theta\sin\varphi = 0 \quad . \tag{A. 14}$$

This equation shows that the third term in Eq. (A. 10) can be ignored in the stationary phase approximation. Consequently, the nuclear scattering amplitude takes the form of

$$f_N(\theta) \sim \frac{2\pi}{ik}\sqrt{\frac{\theta}{\sin\theta}}\left(\frac{\Theta''_{NR}}{2}\right)^{-1/3} e^{2i\delta(\lambda_{NR})}\Big\{p(\theta)J_0(\lambda_{NR}\theta) + iq(\theta)J_1(\lambda_{NR}\theta)\Big\} \quad . \tag{A. 15}$$

We next determine the $p(\theta)$ and $q(\theta)$. Substituting the stationary phase values $\varphi = 0$ ($\phi = 0$) and $\varphi = \pi$ ($\phi = \pi$) into Eq. (A. 9), we obtain

$$p(\theta) + q(\theta) = \lambda_s^- |S(\lambda_s^-)| \mathrm{Ai}\left[\left(\frac{\Theta''_{NR}}{2}\right)^{-1/3}(\theta_{NR} + \theta)\right]\left(\frac{d\phi}{d\varphi}\Big|_{\varphi=0}\right) \tag{A. 16}$$

$$p(\theta) - q(\theta) = \lambda_s^+ |S(\lambda_s^+)| \mathrm{Ai}\left[\left(\frac{\Theta''_{NR}}{2}\right)^{-1/3}(\theta_{NR} - \theta)\right]\left(\frac{d\phi}{d\varphi}\Big|_{\varphi=\pi}\right) \quad . \tag{A. 17}$$

We now consider the property of the mapping $\phi(\varphi)$ to determine the expressions of $\left(\frac{d\phi}{d\varphi}\Big|_{\varphi=0}\right)$ and $\left(\frac{d\phi}{d\varphi}\Big|_{\varphi=\pi}\right)$ in terms of the scattering angle, nuclear rainbow angular momentum and the stationary phase angular momentum. We assume that the following equality holds in the neighborhood of $\phi = 0(\varphi = 0)$ and $\phi = \pi(\varphi = \pi)$

$$\begin{aligned} a(\theta) + b(\theta)\cos\varphi &= 2\delta(\lambda_{NR}) + \lambda_{NR}\theta\cos\phi(\varphi) + \frac{\Theta''_{NR}}{2}(\lambda_s(\theta,\phi(\varphi)) - \lambda_{NR})^3 \\ &+ (\theta_{NR} + \theta\cos\phi(\varphi))(\lambda_s(\theta,\phi(\varphi)) - \lambda_{NR}) \quad . \end{aligned} \tag{A. 18}$$

Partial differentiation of both sides of Eq. (A. 18) with respect to φ leads to

$$\begin{aligned} -b(\theta)\sin\varphi &= \frac{3\Theta''_{NR}}{2}(\lambda_s(\theta,\phi(\varphi)) - \lambda_{NR})^2 \cdot \frac{\partial\lambda_s}{\partial\phi}\cdot\frac{\partial\phi}{\partial\varphi} \\ &+ (\theta_{NR} + \theta\cos\phi(\varphi))\cdot\frac{\partial\lambda_s}{\partial\phi}\cdot\frac{\partial\phi}{\partial\varphi} - \lambda_s\theta\sin\phi(\varphi)\frac{\partial\phi}{\partial\varphi} \quad . \end{aligned} \tag{A. 19}$$

On the other hand, Eq. (5. 12) leads to

$$\frac{\partial\lambda_s}{\partial\phi} = \frac{\mp i\theta\sin\phi}{\sqrt{2\Theta''_{NR}(\theta_{NR} + \theta\cos\phi)}} \approx 0 \quad . \tag{A. 20}$$

The second approximate equality holds because we are considering Eqs. (A. 18) and (A. 19) in the vicinity of the stationary phase positions $\phi = 0$ or π. Using this approximation, we obtain

$$\lambda_s(\theta, \phi(\varphi))\theta \sin\phi(\varphi)\frac{d\phi}{d\varphi} = \lambda_{NR}\theta \sin\varphi \quad , \tag{A. 21}$$

where we replaced the partial differentiation $\frac{\partial\phi}{\partial\varphi}$ by the total differentiation $\frac{d\phi}{d\varphi}$, i.e.

$$\frac{\partial\phi}{\partial\varphi} = \frac{d\phi}{d\varphi} \quad , \tag{A. 22}$$

since the $\phi(\varphi)$ is the one-to-one mapping[9]. Further differentiating both sides of Eq. (A. 21) with respect to φ and using again Eqs. (A. 20) and (A. 22), we obtain

$$\lambda_{NR}\theta\cos\varphi = \lambda_s\theta\cos\phi\left(\frac{d\phi}{d\varphi}\right)^2 + \lambda_s\theta\sin\phi\frac{d^2\phi}{d\varphi^2} \quad . \tag{A. 23}$$

By putting $\phi = 0$ ($\varphi = 0$) or $\phi = \pi$ ($\varphi = \pi$) in Eq. (A. 23), we obtain the derivative of $\phi(\varphi)$ at $\varphi = 0$ and π as,

$$\lambda_s^{\mp}\theta\left(\left.\frac{d\phi}{d\varphi}\right|_{\varphi=0,(\pi)}\right)^2 = \lambda_{NR}\theta \tag{A. 24}$$

$$\left.\frac{d\phi}{d\varphi}\right|_{\varphi=0,(\pi)} = \pm\left\{\frac{\lambda_{NR}\theta}{\lambda_s^{\mp}\theta}\right\}^{1/2} \quad . \tag{A. 25}$$

We choose the positive root in Eq. (A. 25), since it is preferable if $\phi(\varphi)$ increases with φ. Substituting Eq. (A. 25) into Eqs. (A. 16) and (A. 17), we obtain

$$\begin{aligned} p(\theta) &= \frac{1}{2}\sqrt{\frac{\lambda_{NR}\theta}{\theta}}\left[\sqrt{\lambda_s^-}|S(\lambda_s^-)|\mathrm{Ai}\left[\left(\frac{\Theta''_{NR}}{2}\right)^{-1/3}(\theta_{NR}+\theta)\right]\right. \\ &+ \left.\sqrt{\lambda_s^+}|S(\lambda_s^+)|\mathrm{Ai}\left[\left(\frac{\Theta''_{NR}}{2}\right)^{-1/3}(\theta_{NR}-\theta)\right]\right] \end{aligned} \tag{A. 26}$$

$$\begin{aligned} q(\theta) &= \frac{1}{2}\sqrt{\frac{\lambda_{NR}\theta}{\theta}}\left[\sqrt{\lambda_s^-}|S(\lambda_s^-)|\mathrm{Ai}\left[\left(\frac{\Theta''_{NR}}{2}\right)^{-1/3}(\theta_{NR}+\theta)\right]\right. \\ &- \left.\sqrt{\lambda_s^+}|S(\lambda_s^+)|\mathrm{Ai}\left[\left(\frac{\Theta''_{NR}}{2}\right)^{-1/3}(\theta_{NR}-\theta)\right]\right] \quad . \end{aligned} \tag{A. 27}$$

Substituting Eqs. (A. 26) and (A. 27) into Eq. (A. 15), we finally reach the analytic expression of the nuclear scattering amplitude given by Eq. (5. 16).

Finally, we wish to comment on the stationary phase evaluation of the integral over φ in Eq. (A. 10). The function $h(\varphi, \theta)$ contans Airy function Ai as indicated by Eqs. (A. 8) and (A. 9).

It oscillates in the bright region, and could change fairly fast in the shadow region though it is a monotonic function. These properties might affect the stationary phase evaluation of Eq. (A. 10). We defer, however, this problem to future works.

References

[1] A. N. Ostrowski, W. Tiereth and H. Voit, Phys.Rev.**C44** (1991) 2082

[2] D. A. Goldberg and S. M. Smith, Phys. Rev. Lett. **29** (1972) 500

[3] Y. Sugiyama *et al.* Phys. Lett. **B312** (1993) 35

[4] M. E. Brandan, M. S. Hussein, K. W. McVoy and G. R. Satchler, Comm. Nucl. Part. Phys. **77** (1996) 22

[5] N. Takigawa and S. Y. Lee, Nucl. Phys. **A292** (1977) 173

[6] Th. Delbar *et al.* Phys. Rev. **C18** (1978) 1237

[7] K. W. Ford and J. A. Wheeler, Ann. Phys. **7** (1959) 259

[8] M. V. Berry and K. E. Mount, Rep. Prog. Phys. **35** (1972) 315

[9] M. V. Berry, J. of Phys. **B2** (1969) 381

[10] J. Barrette and N. Alamanos, Nucl. Phys. **A441** (1985) 733

[11] C. Marty, Z. Phys. **A309** (1983) 261

[12] W. Treu, H. Fröhlich, W. Galster, P. Dück and H. Voit, Phys. Rev. **C22** (1980) 2462

[13] J. T. Holdeman and R. M. Thaler, Phys. Rev. **139** (1965) B1186
Phys. Rev. Lett. **14** (1965) 81

[14] M. Ueda and N. Takigawa, Nucl. Phys. **A598** (1996) 273

[15] M. Ueda, M. P. Pato, M. S. Hussein and N. Takigawa, Phys. Rev. Lett. **81** (1998) 1809

[16] T. Yamaya *et al*, Phys. Lett. **B417** (1998) 7

[17] L. W. Put and A. M. J. Paans, Nucl. Phys. **A291** (1977) 93

[18] N. Takigawa and L. W. Put, Phys. Lett. **B84** (1979) 371

[19] D. M. Brink and N. Takigawa, Nucl. Phys. **A279** (1977) 159

[20] A. Z. Schwarzchild *et al*, Proc. Conf. on Macroscopic feature of Heavy-ion Collision, 1976 (Argonne National Laboratory, ANL/PHY-76-2) 253

[21] M. Ueda, Doctorate thesis, Tohoku University (1996) unpublished.

[22] M. S. Hussein, Phys. Lett. **B127** (1983) 165

[23] D.M.Brink, *Semi-classical method in nucleus-nucleus scattering* (Cambridge University Press, Cambridge, 1985)

[24] M. A. Abramowitz and I. A. Stegun, *Handbook of Mathematical Functions* Dover Pub. Inc., New York (1965)

[25] N. Rowley and C. Marty, Nucl. Phys. **A266** (1976) 494

[26] M. S. Hussein and K. W. Mcvoy, Prog. Part. Nucl. Phys. **12** (1984) 103 L. van Hove (North-Holland, Amsterdam, 1966) p. 321

[27] W. E. Frahn, *Diffractive Processes in Nuclear Physics* (Oxford University Press, Oxford, 1985)

[28] M. P. Pato and M. S. Hussein, Phys. Rep. **189** (1990) 127

Figure Legends

Figure 1: The σ_{SOD} for the α+^{90}Zr elastic scattering(the solid curve). Parameters of the semiclassical calculation(the dashed curve) are σ_R = 1617 mb, $|f_N(0.02°)|$ = 19.88 fm, arg $f_N(0.02°) = -1.328$ rad. and the frequency of the zeroth order Bessel function = 19.00, respectively.

Figure 2: The deflection functions for the α+^{90}Zr elastic scattering(the solid curve) and for the corresponding Rutherford scattering(the dashed curve). The former is given by Eq. (4. 3) using the phase shifts calculated quantum mechanically. The long-dashed and dot-dashed curves show the deflection functions for the barrier and internal waves, respectively. They have been calculated using the three-turning-points semiclassical formulae for the S-matrices[5, 19].For barrier waves the Coulomb rainbow angle is about 18° at $\lambda \approx 23$ and the nuclear rainbow angle is about 11° at $\lambda \approx 19$. The deflection function for the internal waves looses its physical meaning for angular momenta larger than 40, since there is no potential pocket for those high partial waves.

Figure 3: Reflection coefficients as functions of the angular momentum. The solid, long-dashed and dot-dashed curves are those for the total, the barrier and the internal waves, respectively. The closed circles have been calculated quantum mechanically.

Figure 4: The angular distribution of the modulus of the nuclear scattering amplitude for the α+^{90}Zr elastic scattering at $E_{Lab.}$ = 40 MeV. The solid curve was calculated quantum mechanically, while the dashed and the dot-dashed curves using the semiclassical formulae Eqs. (5. 17) and (5. 18), respectively, where the nuclear rainbow angular momentum $\ell_{NR} = \lambda_{NR} - 1/2$, the curvature of the deflection function at λ_{NR} $\Theta''(\lambda_{NR})$ and the reflection coefficient $|S(\lambda_{NR})|$ have been taken to be 18.6, 0.136 and 0.700, respectively.

Figure 5: Reflection coefficients as functions of the angular momentum for ^{18}O + ^{58}Ni scattering. The bombarding energy is 48.4 MeV in the center of mass system.

Figure 6: The deflection functions for the $^{18}O + ^{58}Ni$ elastic scattering at $E_{c.m.}$ =48.4 MeV(the solid curve) and for the corresponding Rutherford scattering(the dashed curve). The nuclear and Coulomb rainbow angles are about 46° at $\lambda \approx 34$ and about 49° at $\lambda \approx 38$, respectively.

Figure 7: Dependence of the deflection function on the strength of absorption. The scattering system is the same as that in Fig. 6.

Figure 8: Angular distribution of the modulus of the nuclear scattering amplitude for the same system. The solid curve has been calculated quantum mechanically. The dashed curve is the angular distribution of the semiclassical nuclear scattering amplitude given by Eq. (5. 17), where the nuclear rainbow angular momentum λ_{NR}, the nuclear rainbow angle, the curvature of the deflection function at λ_{NR} and the reflection coefficient at λ_{NR} are taken to be 34.4, 46.8°, 0.036 and 0.729, respectively.

Figure 9: Incident energy-dependence of the deflection function for the $\alpha+^{90}Zr$ elastic scattering. The top and bottom figures are for the energy-dependent phenomenological and energy-independent optical potentials[17, 18] shown in Table 1, respectively. The latter has been identified with the phenomenological optical potential at 99.5 MeV.

Figure 10: Incident energy-dependences of the glory angular momentum(the top figure; Fig. 10−A), the derivative of the deflection function(the middle figure; Fig. 10−B) and the reflection coefficient at the glory angular momentum(the bottom figure; Fig. 10−C) for the $\alpha+^{90}Zr$ elastic scattering.

Figure 11: Bombarding energy-dependence of the amplitude of the SOD for the $\alpha+^{90}Zr$ elastic scattering. The closed and open circles have been obtained from quantum mechanical calculations for the energy-dependent phenomenological and energy-independent optical potentials, respectively. The solid and dashed curves were calculated by Eqs. (7. 11) and (7. 10), respectively. The dotted and dot-dashed curves were obtained by assuming $E^{1/4}(1 - V_B/E)^{3/4}$ and $E^{1/4}$ behaviours.

Figure 12: Critical energy for the genuine forward nuclear glory scattering. The top figure shows the dependence of the fitting parameter c_1 on the normalization energy. The bottom figure shows the corresponding χ^2 value calculated by Eq. (7. 13). The system is α+^{90}Zr scattering. The 9 energies in Table 1 have been chosen as the normalization energy. The resultant critical energy is indicated by the vertical dashed line.

Table 1: Optical potential parameters for the elastic α+^{90}Zr scattering at each bombarding energy and those for the elastic ^{18}O + ^{58}Ni scattering at $E_{c.m.}$ = 48.4 MeV. The potential form is given by $U(r) = -V_0 f[(r - R_0)/a_0] - iW_0 f[(r - R_W)/a_W]$ with $f[x] = [1 + \exp(x)]^{-1}$. The values of parameters with upper suffices a), b) and c) are taken from Refs. [16], [17] and [19], respectively.

	$E_{Lab.}$	V_0 (MeV)	R_0 (fm)	a_0 (fm)	W_0 (MeV)	R_W (fm)	a_W (fm)
α+^{90}Zr	40.0 MeV[a)]	112.3	6.619	0.524	15.28	6.973	0.344
	59.1 MeV[a)]	120.6	6.054	0.676	20.60	6.794	0.572
	79.5 MeV[a)]	141.2	5.490	0.821	18.49	7.058	0.565
	99.5 MeV[a)]	133.3	5.535	0.805	19.63	7.040	0.562
	118.0 MeV[a)]	124.4	5.624	0.792	20.55	7.036	0.566
	141.7 MeV[a)]	118.3	5.660	0.787	20.84	7.009	0.573
	200.0 MeV[b)]	105.0	5.579	0.801	19.30	7.036	0.567
	250.0 MeV[b)]	93.12	5.579	0.801	20.64	7.036	0.567
	300.0 MeV[b)]	80.70	5.579	0.801	20.93	7.036	0.567
^{18}O+^{58}Ni	63.4 MeV[c)]	100.0	7.790	0.55	20.0	7.790	0.55

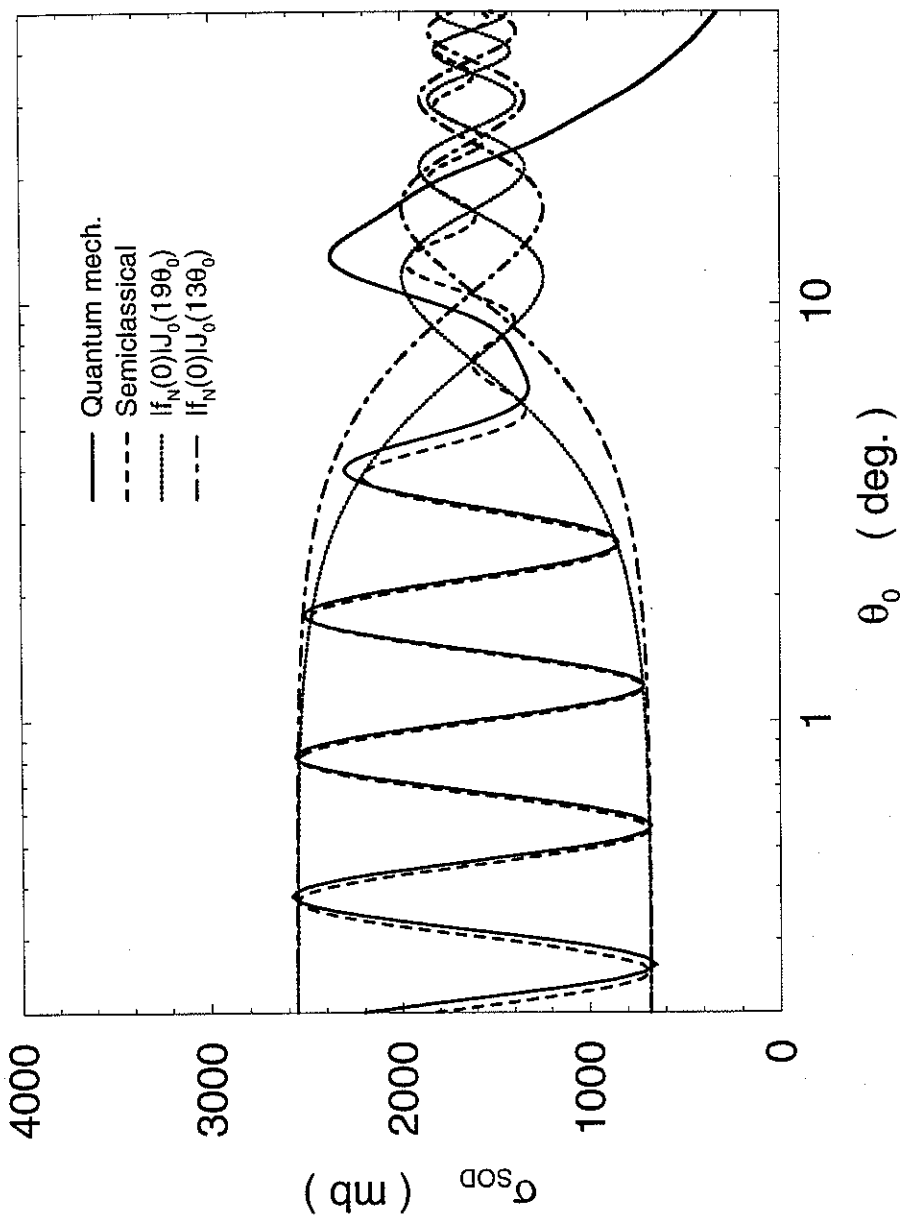
Fig. 1
Quantum mech.
Semiclassical
$|f_N(0)|J_0(19\theta_0)$
$|f_N(0)|J_0(13\theta_0)$
σ_{sob} (mb)
4000
3000
2000
1000
0
1
10
θ_0 (deg.)

Figure 1:

Fig. 2

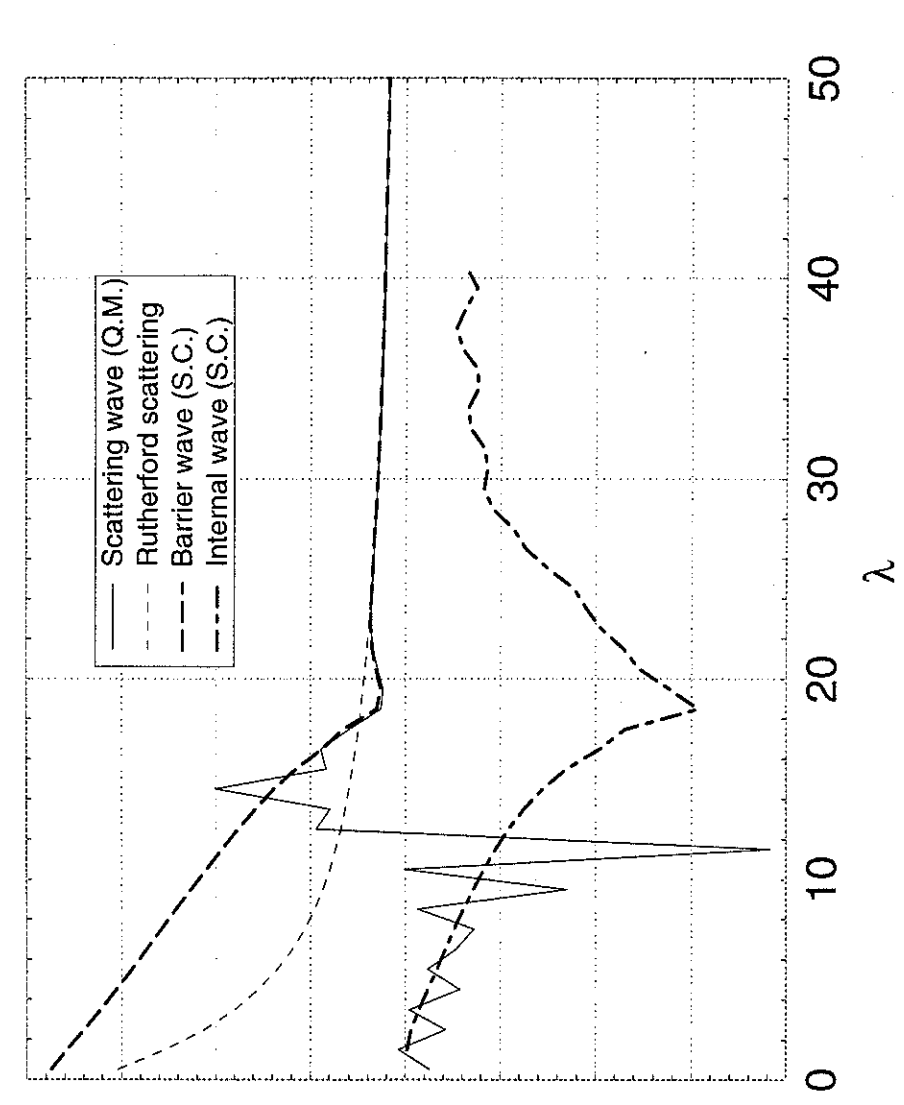

Figure 2:

Fig. 3

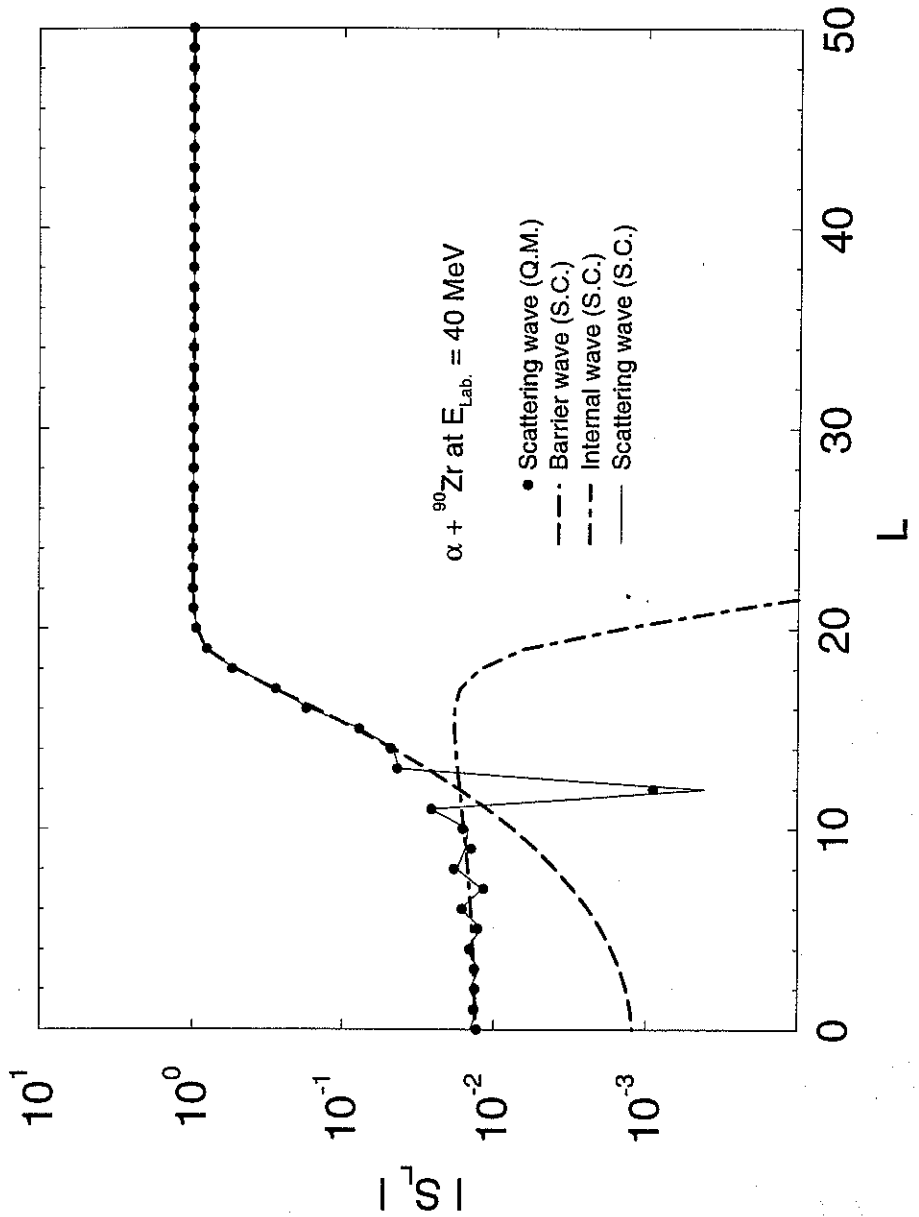

Figure 3:

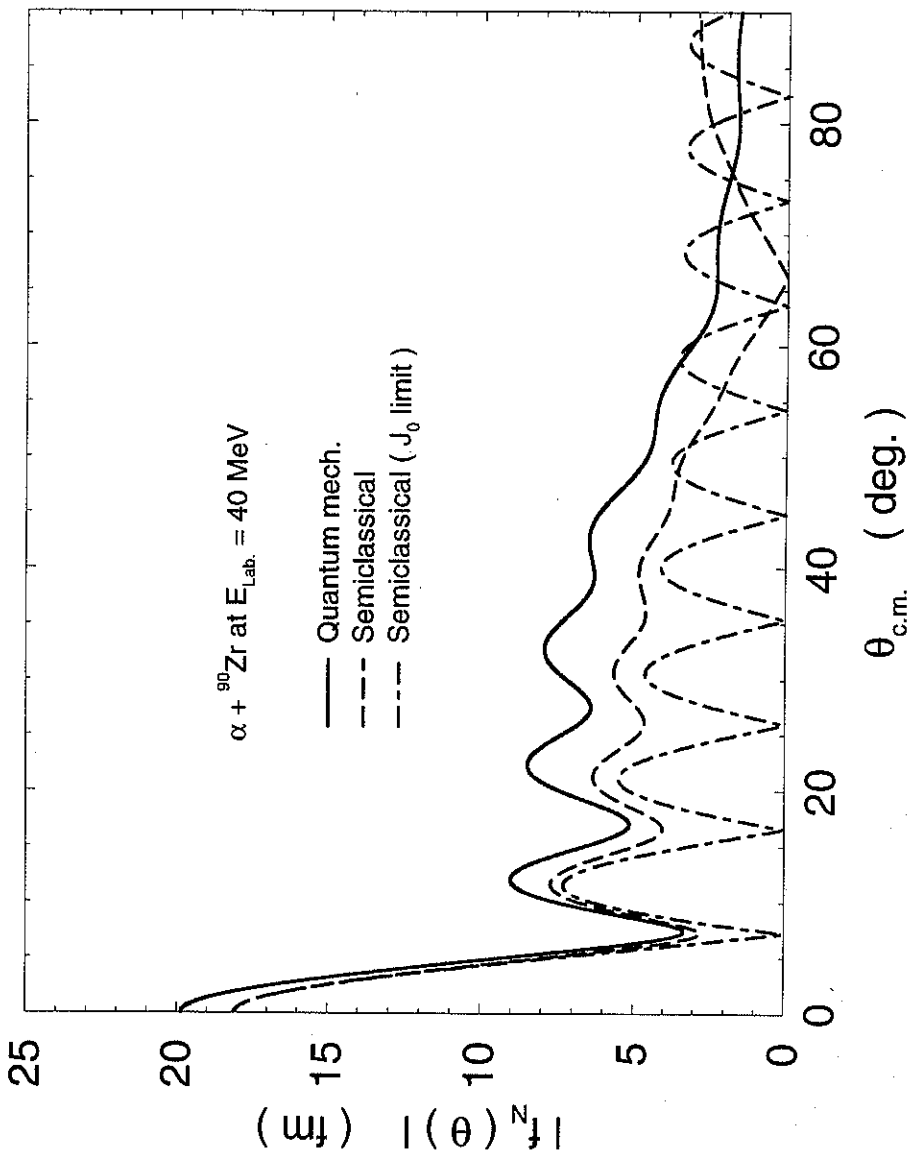
Fig. 4
α + 90Zr at E_Lab. = 40 MeV
Quantum mech.
Semiclassical
Semiclassical (J0 limit)
| f_N (θ) | (fm)
θ_c.m. (deg.)
0
5
10
15
20
25
0
20
40
60
80

Figure 4:

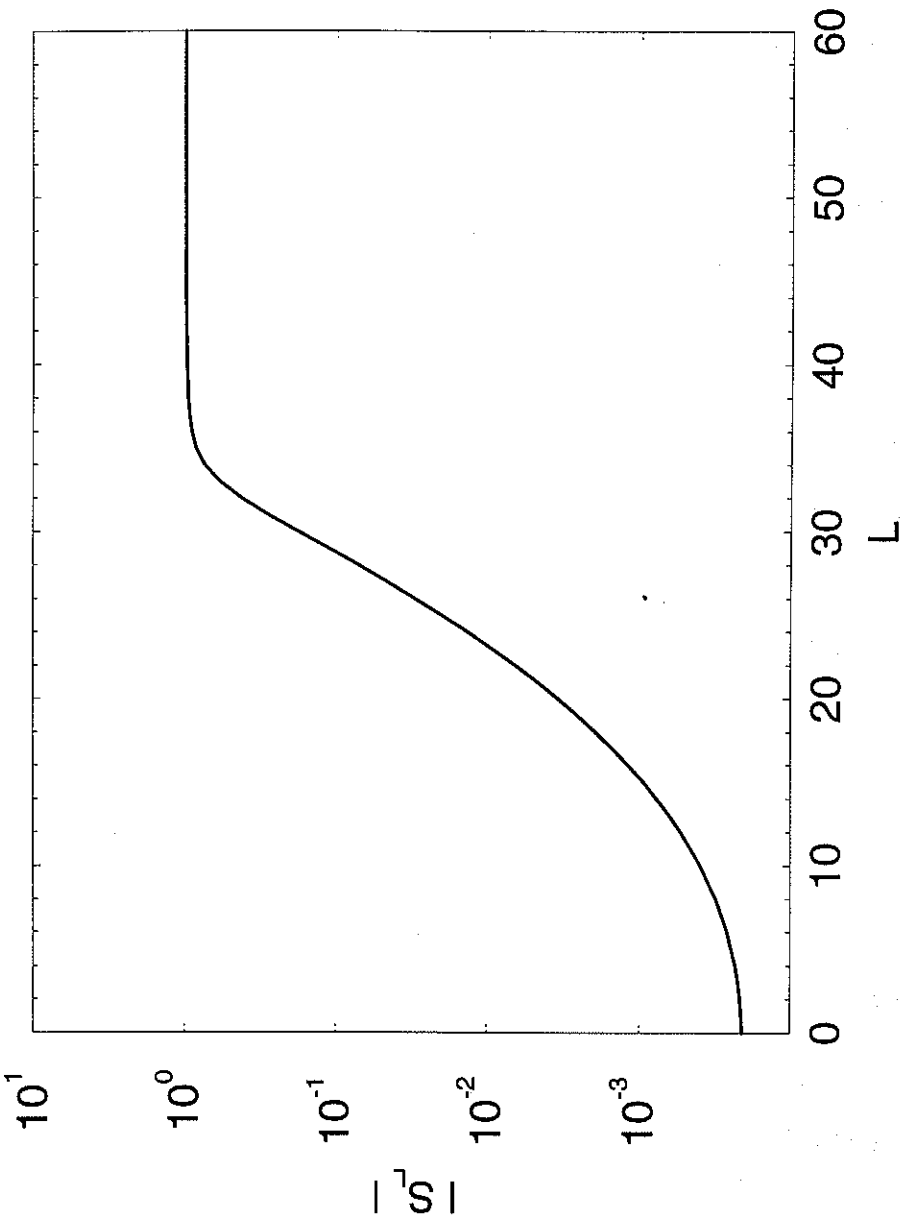

Figure 5:

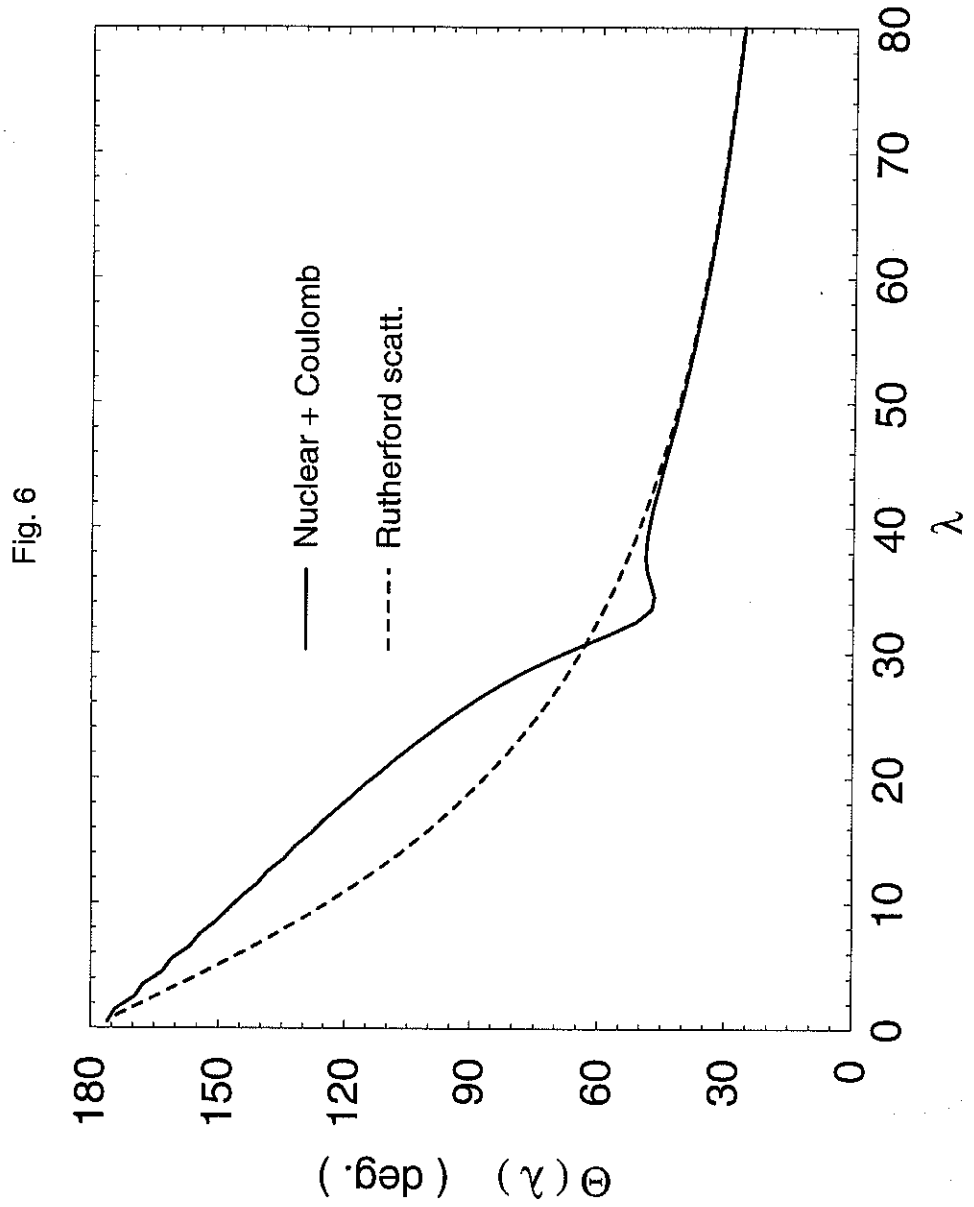
Fig. 6
Nuclear + Coulomb
Rutherford scatt.
Θ (λ) (deg.)
λ
180
150
120
90
60
30
0
0
10
20
30
40
50
60
70
80

Figure 6:

Fig. 7

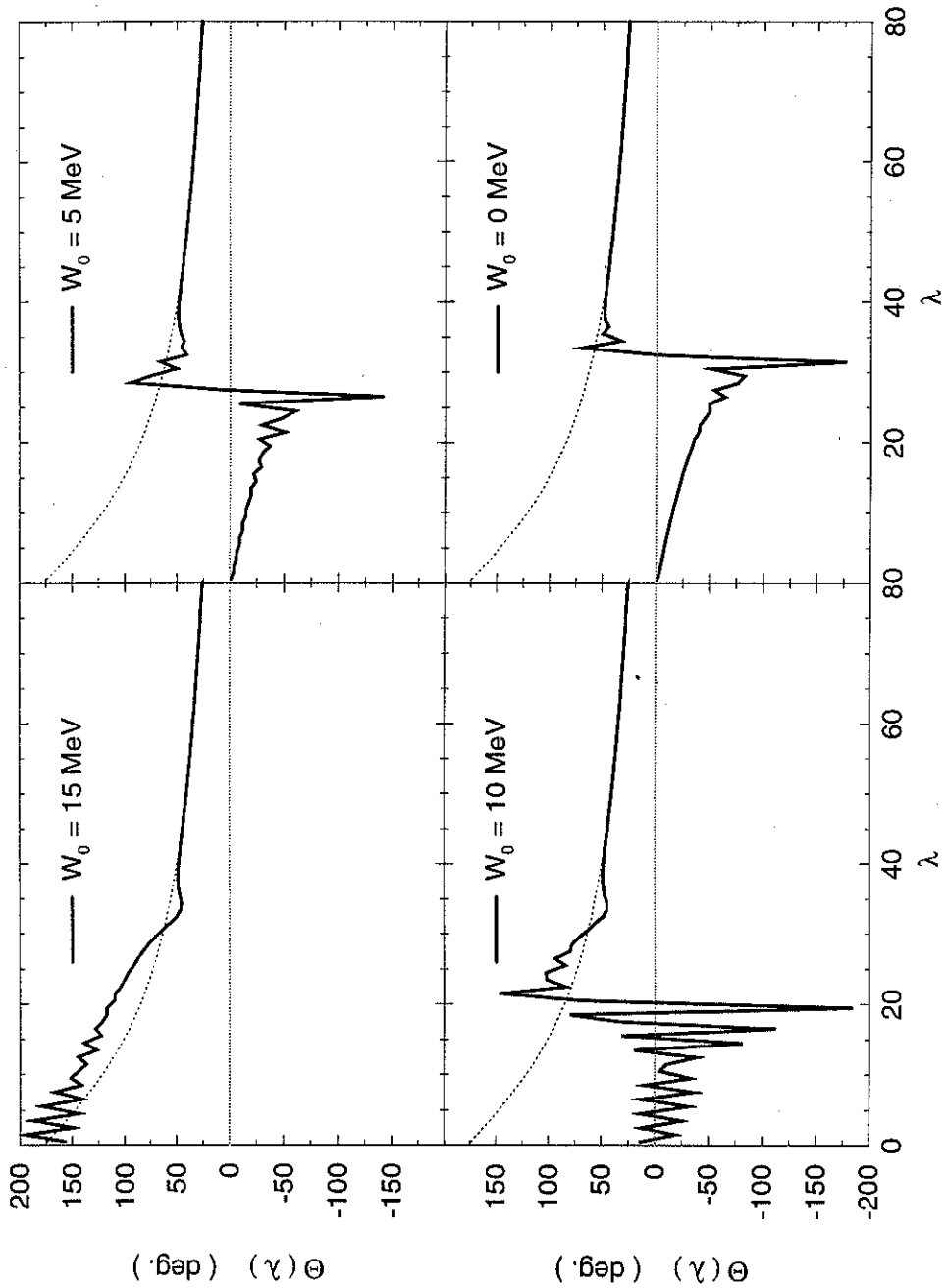

Figure 7:

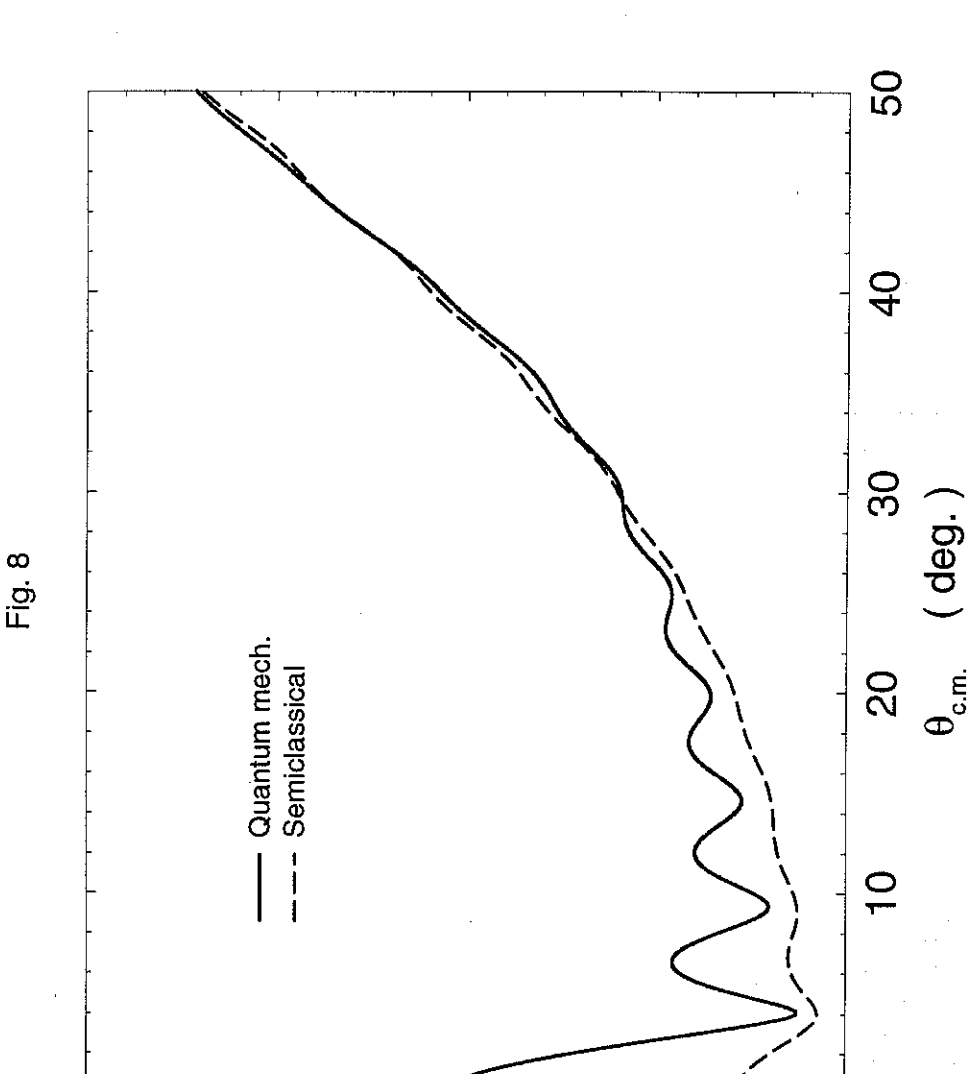
Fig. 8
Quantum mech.
Semiclassical
$|f_N(\theta)|$ (fm)
$\theta_{c.m.}$ (deg.)
0.0
1.0
2.0
3.0
4.0
0
10
20
30
40
50

Figure 8:

Fig. 9

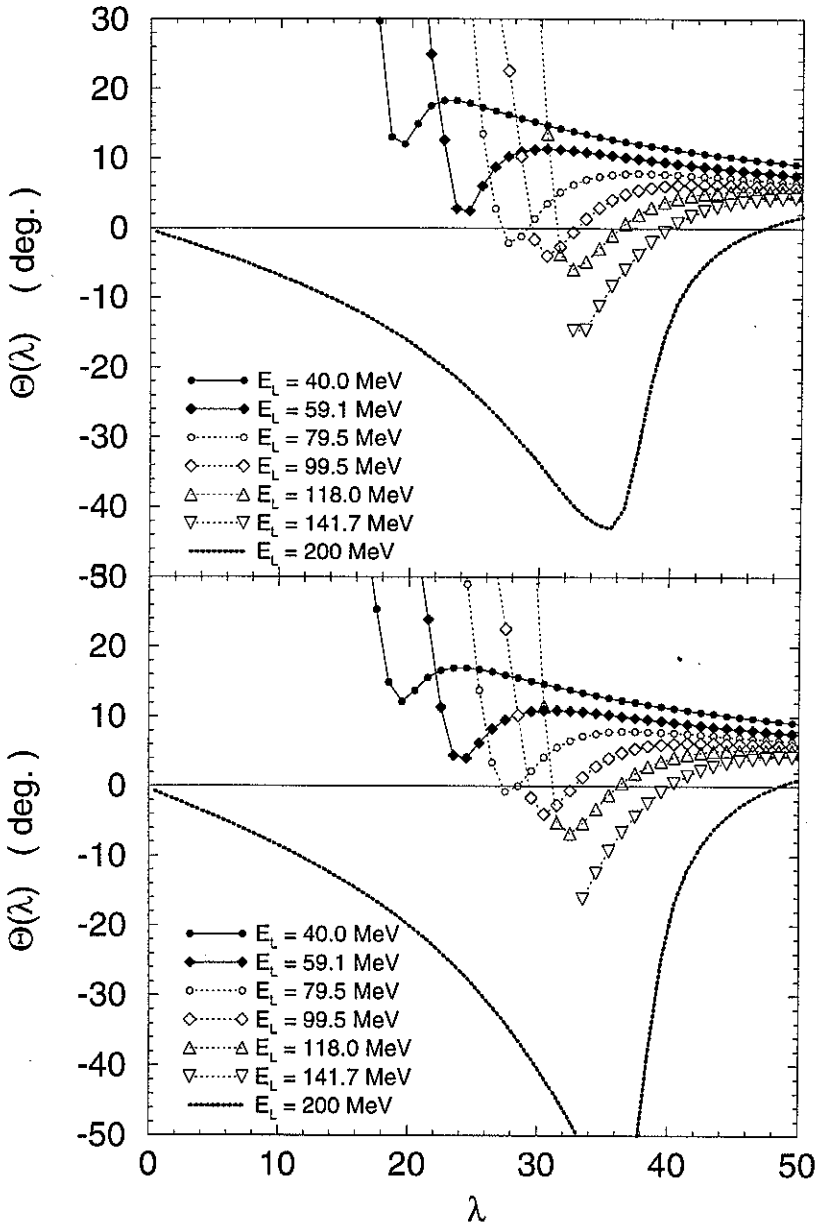

Figure 9:

Fig. 10

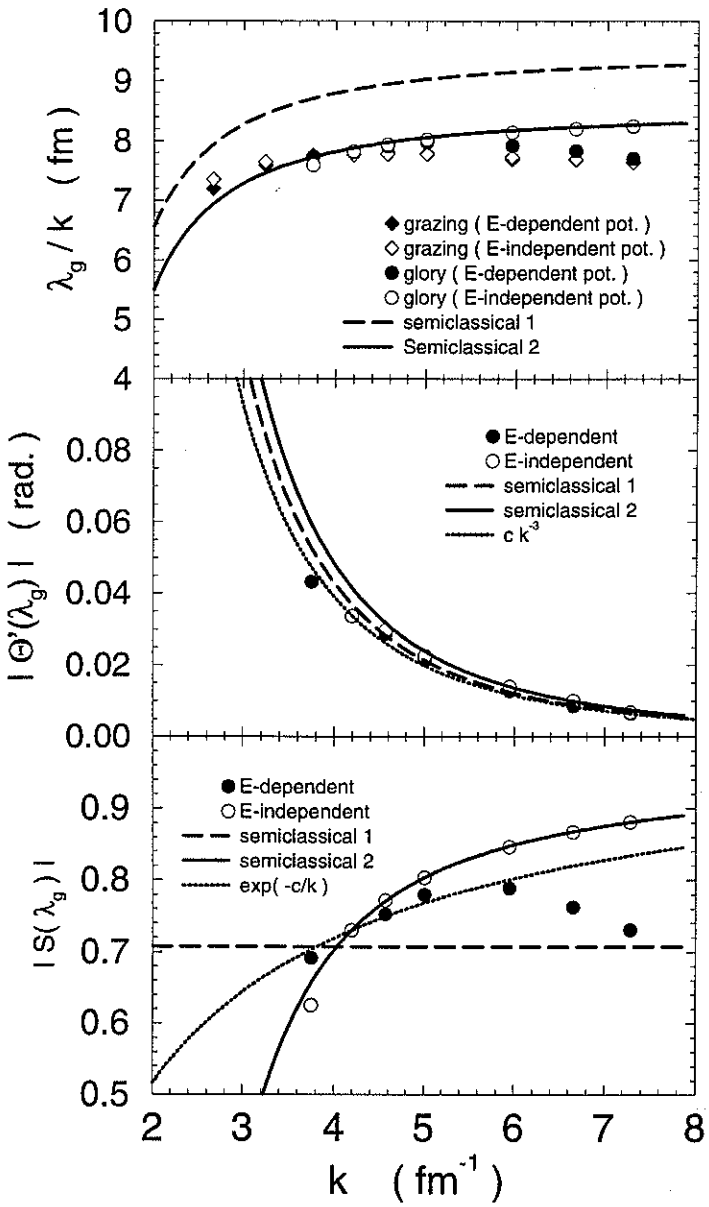

Figure 10:

Fig. 11

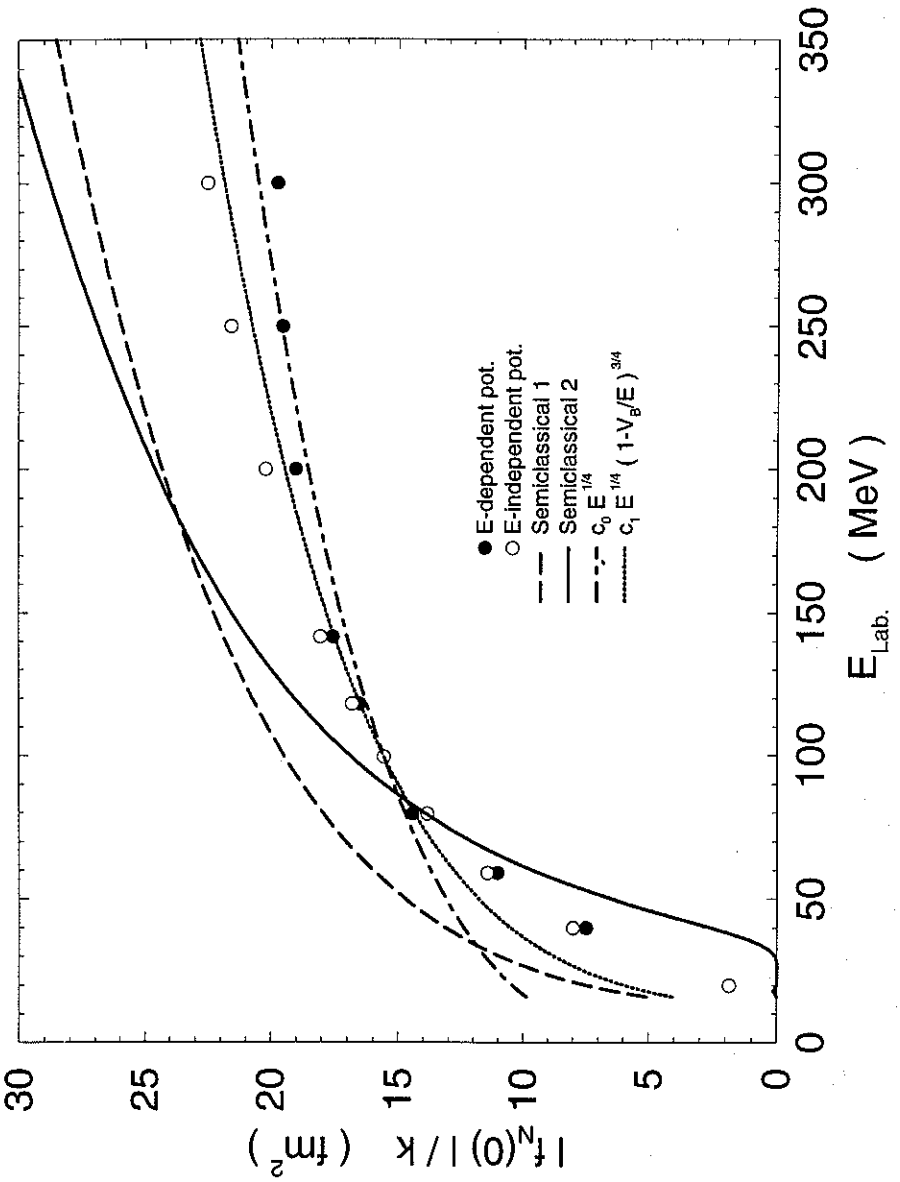

Figure 11:

Fig. 12

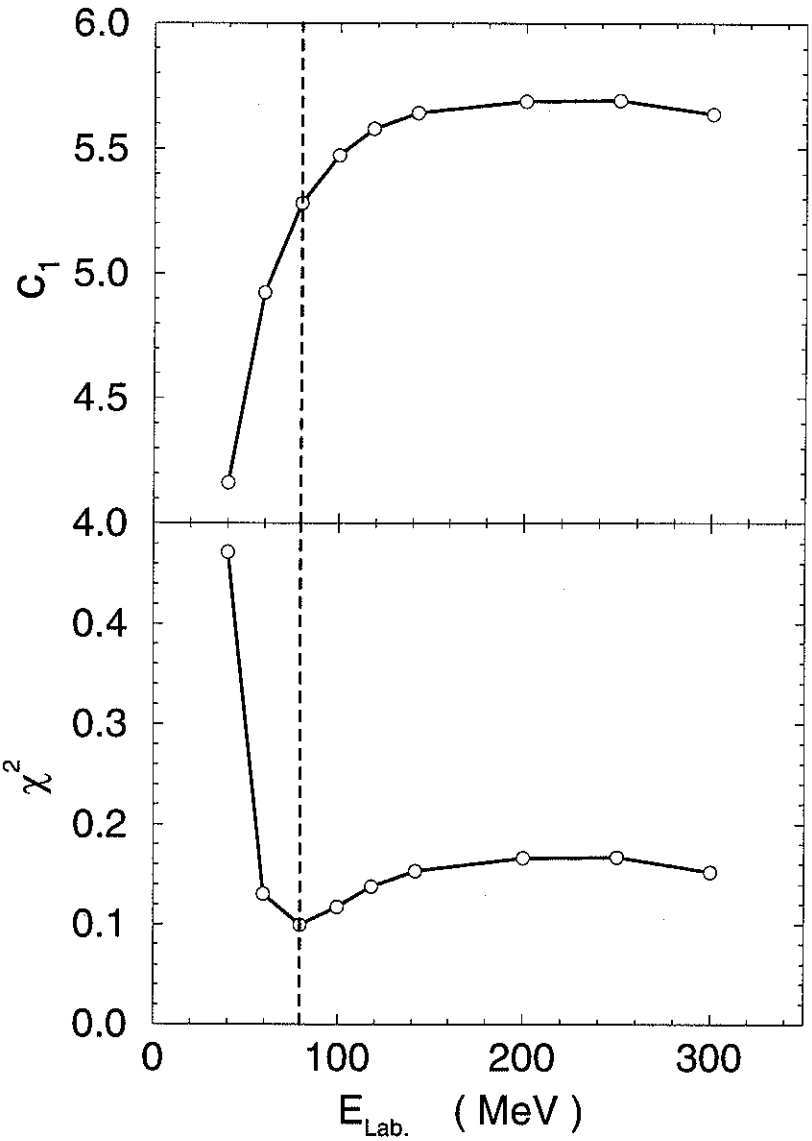

Figure 12: